

# DAMAGE DETECTION IN CARBON FIBER REINFORCED POLYMERS USING ACOUSTIC EMISSION

– “Detecting matrix cracks in cross-ply layups.”

**Magnus Snällfot**

**Simon Lidman**

**Carl Liljeberg**

Supervisor: Johan Hedbrant

Examiner: Jonas Detterfelt



## Abstract

Currently, the only way of reliably detecting damage in composites is through optical analysis through a microscope. This manual process is very time-consuming and may even be impossible if the quantity of cracks is high enough. Additionally, optical analysis is not possible in real world applications without dismantling the structure or sometimes cutting into the object, permanently destroying it. Acoustic emission (AE) as a structural health monitoring (SHM) tool offers to solve this problem by providing a faster, less intrusive method of damage analysis.

In this bachelor's thesis, it was investigated how an AE system would be constructed, the effectiveness of it, and what are the challenges associated with it. The development of this AE system was made in mind of replacing the traditional optical analysis completely or partially, using cross-ply carbon fiber reinforced polymer made in-house by a fellow student group at Linköping University. Despite having aspired to do many more tests, and the data set being relatively small, a process was developed which would serve as the backbone of an AE system. The process involves data collection through piezoelectric sensors, signal filtering, and matrix crack calculations based on known parameters and data processing. Overall, the system was successful but requires more investigation and testing to provide information about accuracy and effectiveness.

## Preface

Special thanks to Leif Norman, Johan Hedbrant, and Mohamed Loukil for your support and for helping us solve problems that would otherwise make this project impossible.

This thesis is written in collaboration by three student writers with the following distribution of field efforts:

Field	Magnus S	Simon L	Carl L
Preparation work and planning	50%	25%	25%
Literature study and collection	40%	25%	35%
Software tweaking and investigation	30%	40%	30%
Hardware research and purchases	35%	35%	30%
Data Analysis	30%	30%	40%
Matlab script coding and data presentation	0%	70%	30%
Illustrations	0%	0%	100%
Theory writing	40%	25%	35%
Method writing	30%	40%	30%
Results writing	30%	30%	40%
Discussion and conclusion writing	40%	30%	30%

## Table of Contents

Abstract.....	i
Preface.....	ii
Table of figures .....	v
Nomenclature .....	vii
1 Background .....	1
2 Introduction .....	2
2.1 Aim .....	2
2.2 Research questions.....	2
2.3 Delimitations .....	2
2.4 Target audience.....	2
2.5 Ethics and society .....	2
3 Research strategy and process .....	3
4 Theory.....	4
4.1 Acoustic emission theory.....	4
4.1.1 Principle of acoustic emission for damage detection .....	4
4.1.2 Hit-based AE methodology .....	4
4.1.3 Piezoelectric sensor.....	7
4.1.4 Sensor coupling .....	7
4.1.5 Hsu-Nielsen source.....	7
4.1.6 Energy attenuation phenomena .....	8
4.1.7 Influence of different sensors .....	8
4.2 Damage mechanisms in CFRP.....	8
4.2.1 Debonding.....	8
4.2.2 Matrix crack.....	8
4.2.3 Delamination.....	8
4.2.4 Fiber breakage.....	9
4.3 Peak frequency signals from matrix cracks .....	9
4.4 Linear correlation between matrix crack density and cumulative AE energy .....	10
4.5 Damage localization techniques.....	11
5 Experimental methodology .....	12
5.1 Tensile machine.....	12
5.2 Acoustic emission sensor.....	12

5.3	Acquisition setup .....	12
5.4	CFRP testing specimen .....	13
5.5	Experimental setup.....	16
5.6	Hsu-Nielsen source testing .....	16
5.7	Testing .....	17
5.7.1	Incremental load increase.....	17
5.8	Detecting matrix cracks using microscope .....	17
5.9	Data analysis.....	18
5.9.1	Damage mechanism definition .....	18
6	Results & Analysis .....	19
6.1	Cumulative hits vs tensile stress.....	19
6.2	Cumulative energy vs stress .....	20
6.3	Peak frequency results .....	24
6.4	Matrix crack data.....	25
6.5	Cumulative energy to describe amount of matrix cracks .....	26
6.6	Example of implementation of cumulative energy to predict cracks vs stress .....	29
7	Discussion .....	32
7.1	Automating filter algorithms .....	32
7.2	Why multiple sensors might be necessary .....	32
7.3	Sources of errors .....	33
7.4	Limitations of cumulative energy to predict number of matrix cracks .....	33
7.5	Future experimental improvements .....	34
8	Conclusions .....	35
9	References .....	36
10	Appendix.....	39

## Table of figures

Figure 1: The principle of acoustic emission. Inspired by [3].....	4
Figure 2: Explanation of timing parameters. Inspired by [5] .....	5
Figure 3: Explanation of features. Inspired by [8].....	6
Figure 4: Explanation of how peak frequency is computed. Inspired by [7].....	7
Figure 5: (a) Debonding. (b) Matrix crack. (c) Delamination between 0° and 90° layers. (d) Fiber breakage. [13].....	9
Figure 6: Displays difference between inner and outer 90° plies. ....	10
Figure 7: The acquisition setup. The USB AE Node is connected to a computer, where data is computed and stored. The connector seen at the bottom of the picture is connected to the tensile machine to measure the load.....	13
Figure 8: Displays the layup on the specimens used in the experiments. ....	14
Figure 9: Specimen without tabs adhered (left) and specimen with tabs adhered (right).....	15
Figure 10: Specimen with indentation from tensile machine (a) and line that show where gauge length start was measured when mounted (b). .....	15
Figure 11: Experimental setup. The specimen is mounted in the tensile machine and the sensor is held fixed onto the specimen with a clamp.....	16
Figure 12: Cumulative hits vs stress for all tests made. Legend: tests 1 – 14, total stress accumulation..	19
Figure 13: Percentage of cumulative hits against time after pullstop. Legend: tests 1 – 14, total stress accumulation. ....	20
Figure 14: Cumulative energy vs stress for all tests. Legend: tests 1 – 14, total stress accumulation. ....	21
Figure 15: Cumulative hits vs stress for all tests after filtering out hits with higher energy than $1.5 * 10^7 \text{ aJ}$ . Legend: tests 1 – 14, total stress accumulation.....	21
Figure 16: Energy derivative vs stress. Legend: tests 1 – 14, total stress accumulation. tests 1 – 14, total stress accumulation.....	22
Figure 17: Percentage of cumulative energy against time after pullstop. Legend: tests 1 – 14, total stress accumulation. ....	23
Figure 18: Percentage of cumulative energy against time after pullstop after filtering out hits with higher energy than $1.5 * 10^7 \text{ aJ}$ . Legend: tests 1 – 14, total stress accumulation. ....	23
Figure 19: Duration vs time of test 13 as an example. Collection time indicated by red line.....	24
Figure 20: Amplitude (y, dB) vs peak frequency (x, kHz). Each dot indicates one hit. Some tests with duplicate maximum stress were excluded. ....	25
Figure 21: Amount of Matrix cracks observed optically under microscope vs amount of total energy recorded with AE setup. ....	27
Figure 22: Amount of Matrix cracks observed optically under microscope vs amount of total energy recorded with AE setup. High energy events are filtered out. ....	27
Figure 23: Amount of Matrix cracks observed optically under microscope vs amount of energy recorded up until pullstop with AE setup.....	28
Figure 24: Amount of Matrix cracks observed optically under microscope vs amount of energy recorded up until pullstop with AE setup. High energy events are filtered out.....	28
Figure 25: Average number of matrix cracks per side of the specimen vs the accumulated energy at pullstop. ....	29
Figure 26: Accumulated acoustic energy vs max stress. With a second-degree polynomial fit. ....	30

Figure 27: Average number of matrix cracks per side vs max stress. Points with optically counted cracks and the calculated function of the expected number of cracks. ....	30
Figure 28: Average number of matrix cracks per side vs max stress. Points with optically counted cracks and the calculated function of the expected number of cracks. With two other points.....	31

## Nomenclature

AE – Acoustic Emission

CF – Carbon Fiber

CFRP – Carbon Fiber Reinforced Polymer

SHM – Structural Health Monitoring

FFT – Fast Fourier Transform

UD – Uni-Directional

AE event – Elastic waves that are generated from the same damage source

Hit – Part of a waveform defined by a threshold and timing parameters

Pullstop – Point at which maximum stress is achieved during a tensile test

Cross-ply – Layup with only two perpendicular fiber directions, such as  $[0^\circ, 90^\circ, 0^\circ, 90^\circ]$ s

## 1 Background

Hydrogen can be used as an alternative fuel source to decrease greenhouse gas emissions and fossil fuel dependency. Because of its low volumetric energy density, it needs to be stored in high pressure tanks to be a viable fuel option, often in utilization where movement is involved.

Today the vessels used for storage of high-pressure hydrogen are full-metal tanks, metal tanks reinforced by composites or composite tanks with or without plastic lining, where the latter is the most appealing for use in avionics, automotive and transportation since it is the lightest option. During operation, composite tanks are subject to loads that could lead to damage. This damage has potential to compromise the structural integrity and performance of the tanks, leading to gas leakage or rupture.

Structural health monitoring (SHM) of composite hydrogen tanks is desirable to ensure reliable and safe use. One technique used in SHM is the acoustic emission (AE) method. The AE method uses sensors to detect elastic waves formed from a sudden release of strain energy that propagates throughout the material [1]. Hypothetically, the benefit of using AE as a SHM method is the ability to recognize the type, severity, and location of damage in a non-intrusive manner [2].

## 2 Introduction

### 2.1 Aim

In this paper, we aim to evaluate the viability and reliability of the acoustic emission (AE) method on carbon fiber reinforced polymer (CFRP).

### 2.2 Research questions

- How can AE give information about the amount of matrix cracks in cross-ply CFRP?
- What are the main limitations of an AE system?

### 2.3 Delimitations

- The only damage mode considered is matrix cracks in CFRP.
- Only cross-ply laminates for research purposes are examined in substitution of common industry standard quasi-isotropic laminates.
- Only tensile testing is conducted.

### 2.4 Target audience

The target audience is limited to an academic level of bachelor's in mechanical engineering or above.

### 2.5 Ethics and society

This thesis investigates the use of acoustic emission, and therefore the information from this thesis might be a part of the development of a SHM system in the future. Because of this, it's vital that limitations and errors are properly discussed and investigated so that a reader understands how to interpret the results. The reliability of acoustic emission needs to be fully understood, since misunderstandings could lead to the development of an unreliable SHM system, and if used for safety critical infrastructure this might lead to consequences regarding the safety for society. Therefore, this thesis will include a large focus on errors, limitations and reliability of the results and proposed methods. On the other hand, this study could contribute to the implementation of a SHM system for monitoring of, for example, hydrogen tanks. Not only can this lead to improvement regarding safety, but also aid the process of replacing fossil fuels with hydrogen.

### 3 Research strategy and process

Since the topic on AE is not particularly newly discovered or developed, the process of research for this study will be that of trying to understand what has already been done in this field using relevant keywords on databases such as Google Scholar. Gathering information of the highest quality is necessary to avoid excess time investment. To achieve a high enough standard, the research process will incorporate ranking the credibility of a source by valuing a larger number of citations, a newer publication date and larger number of publications by the target author. It is equally important to determine the inherent bias and conflict of interest of an author which must be investigated by accumulating knowledge about the authors' additional ventures and investments. Not considering this possibility might create skewed and/or inaccurate data which in turn becomes detrimental to this study's results. One such bias might be discovered by going through the article's reference list and identifying patterns which would indicate bias, such as excluding important and obvious perspectives. Another way would be to check for misrepresentation of a given reference.

#### **Keywords used:**

- Acoustic emission
- Polymer composites
- CFRP
- Hydrogen tanks

#### **Databases used:**

- Google scholar
- Science
- Scopus

## 4 Theory

This chapter includes theory about acoustic emission (AE) and damage types in composites.

### 4.1 Acoustic emission theory

#### 4.1.1 Principle of acoustic emission for damage detection

The principle of acoustic emission is to measure elastic waves caused by damage within a material [1]. A piezoelectric sensor is often used, which records the elastic waves and transforms them into electrical signals [1]. These signals are analog and are amplified by a pre-amplifier [2]. After the amplification, digital signals are obtained by an acquisition device [2]. Figure 1 displays the principle of acoustic emission. In this paper, an AE event refers to the elastic waves that are generated from the same damage source.

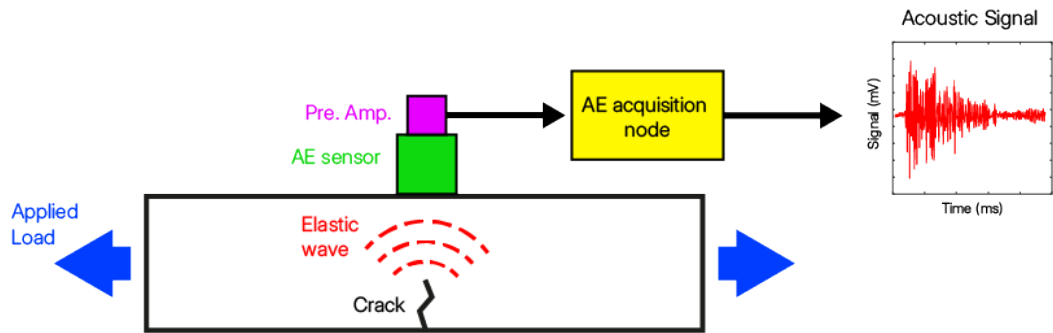


Figure 1: The principle of acoustic emission. Inspired by [3]

#### 4.1.2 Hit-based AE methodology

A signal processing method is necessary to convert the electrical signals into interpretable information, where a hit-based method is a commonly used. This method is completely automated, and the goal is to save separated fractions of the electrical signals of interest while ignoring the rest of the signals. Each fraction is called a hit. Features, describing the characteristics of each hit, is the information used in the analysis. Before acquiring signals, a threshold and three timing parameters must be selected. The threshold needs to be greater than the noise level to exclude noise from the analysis. A hit starts at the first threshold crossing and is then defined by the timing parameters. [4]

The timing parameters are:

- **PDT** (peak definition time,  $\mu\text{s}$ ): This parameter affects the defined amplitude peak of the hit and “is the time after the peak amplitude that the system attempts to determine a new peak amplitude. After the PDT has expired, the original peak amplitude will not be replaced.” [5, p.14]
- **HDT** (hit definition time,  $\mu\text{s}$ ): The duration of the hit is decided by the HDT and is “the time after the last threshold exceedance when the hit is ended” [5, p.14].
- **HLT** (hit lockout time,  $\mu\text{s}$ ): Corresponds to a dead time where new hits can’t be detected [5]. “A new hit can only be started after both the HDT and the HLT have expired” [5, p.14].

Figure 2 explains how the timing parameters work.

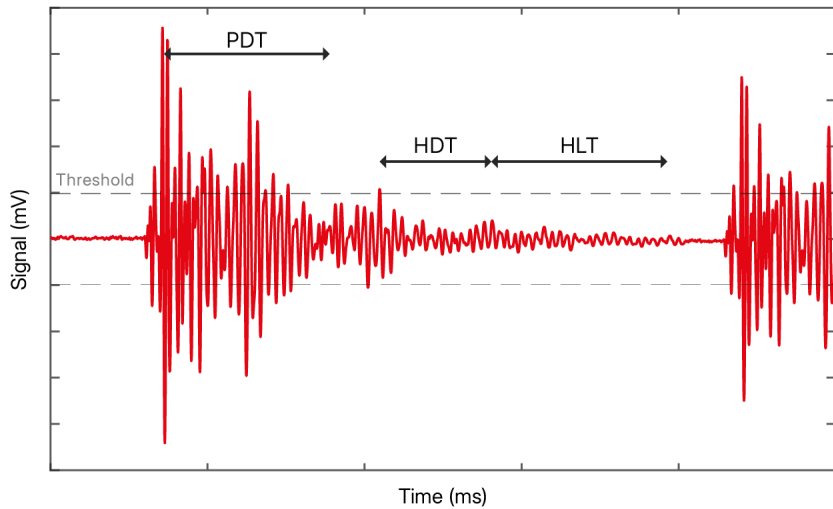


Figure 2: Explanation of timing parameters. Inspired by [5]

Errors in the computation of the hits amplitude peak are avoided by selecting a suitable PDT [6]. When selecting the HDT, one wants to avoid a single AE event being identified as several hits which can be prevented by increasing the HDT [7]. The drawback of extending the HDT is the increased probability of multiple AE events being counted as one hit [7]. Similarly, the choice of HLT is a consideration between using a longer HLT to minimize hits caused by reflections from an already recorded AE event and reducing the HLT to prevent data loss since new AE events could be obtained during this time period [7]. The USB AE node, the acquisition device used in this study, has a manual [6] with recommended values of these timing parameters depending on type of material, see Table 1.

Table 1: Recommended timing parameter values ( $\mu\text{s}$ ). From USB AE node manual [6]

	<b>PDT (<math>\mu\text{s}</math>)</b>	<b>HDT (<math>\mu\text{s}</math>)</b>	<b>HLT (<math>\mu\text{s}</math>)</b>
<i>Composites, non-metals</i>	20–50	100–200	300
<i>Small metal specimens</i>	300	600	1000
<i>Metal structures (high damping)</i>	300	600	1000
<i>Metal structures (low damping)</i>	1000	2000	20 000

Features are used to describe each hit [4]. Saeedifar and Zarouchas [2] defines some of these features as:

- Amplitude: The maximum voltage of the signal and it is usually reported in dB unit.
- Duration: The time interval between the first and the last threshold crossings and it is reported in  $\mu$ s unit.
- Rise time: The time interval between the first threshold crossing and the maximum amplitude and it is reported in  $\mu$ s unit.
- Counts: The number that the waveform crosses the threshold in the increasing direction within the waveform's duration.
- Energy: The area beneath the squared waveform within the waveform's duration. It is usually reported in attojoule (aJ) unit ( $1 \text{ aJ} = 10^{-18} \text{ J}$ ).
- Peak frequency: The frequency corresponded to the highest magnitude in the frequency distribution obtained from fast Fourier transform (FFT) of the signal. It is reported in kHz unit. [2, p. 3]

Figure 3 and Figure 4 shows how most of these features are computed.

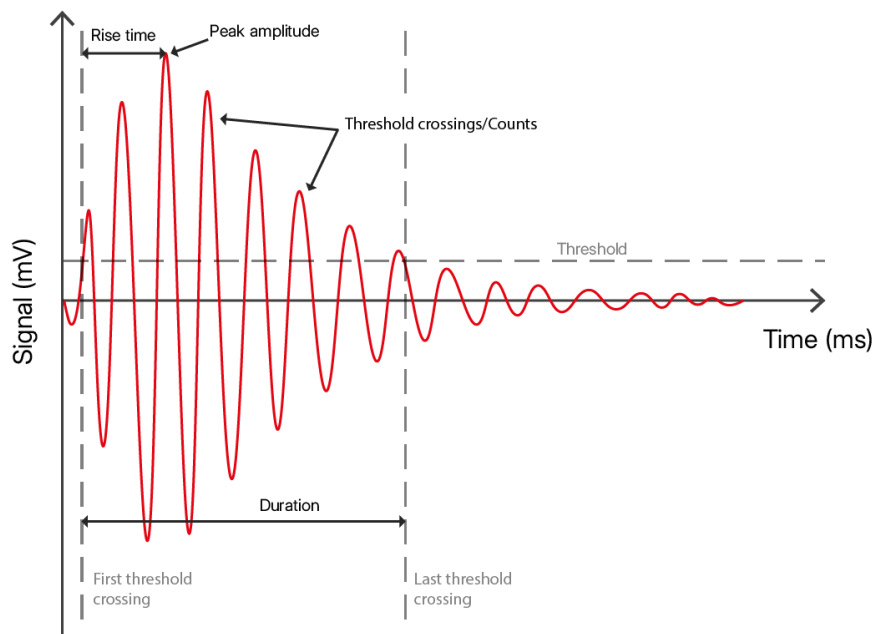


Figure 3: Explanation of features. Inspired by [8]

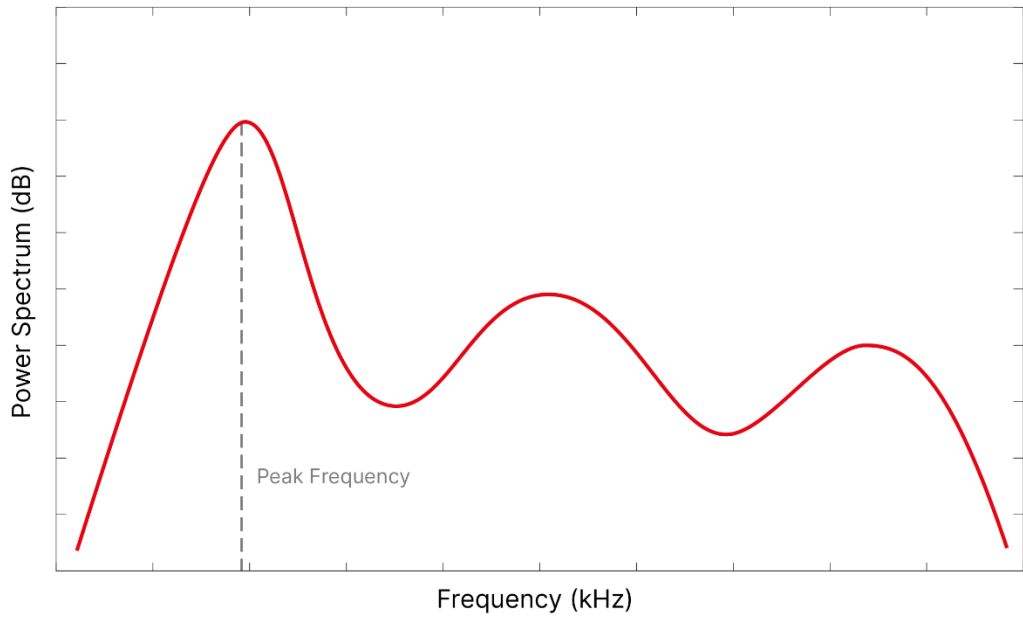


Figure 4: Explanation of how peak frequency is computed. Inspired by [7]

#### 4.1.3 Piezoelectric sensor

Piezoelectricity is a phenomenon where certain solid materials generate electric charges under mechanical stress. This effect is then used to measure changes in force, pressure, acceleration, temperature, and strain. In this study, a thin crystal plate is used to detect high frequency, low amplitude AE due to its sensitivity to such signals.

#### 4.1.4 Sensor coupling

To ensure a good reading of an AE event it is crucial that the medium between the sensor and the specimen of interest does not impede the transmission of the signal. Gel, liquid and grease are examples of coupling mediums used to minimize signal loss. [9]

#### 4.1.5 Hsu-Nielsen source

The Hsu-Nielsen source method evolves around creating an artificial AE source to evaluate the acoustic contact between the sensor and the specimen. The test involves pressing an extended lead from a mechanical pencil on the surface of a specimen until it breaks. The recorded amplitude of the AE signal from each break needs to be above a reference value to confirm proper acoustic contact. [10]

#### 4.1.6 Energy attenuation phenomena

Energy attenuation is the phenomena that creates AE signal loss when an AE signal propagates through a medium. Regarding CFRP, acoustic attenuation is an especially important phenomena to consider because of the relatively high attenuation of AE signals in this material. Because of this feature, attenuation has more impact on the collected signals amplitude, frequency, and signal quality the larger the distance is between the source and the sensor. [11]

#### 4.1.7 Influence of different sensors

Hamam *et al.* [12] found that using different sensors can have a big impact on the obtained frequency content of signals. They compared two different sensors, one with a sensitivity range of 200 - 900 kHz and the other with 500 - 1850 kHz, by placing them on the same position but on opposite sides of a composite specimen in a tensile test. The results showed that the first mentioned sensor primarily labeled signals with a peak frequency of 350 kHz, while the other sensor displayed signals with 600 kHz peak frequency. This indicates that sensor choice has a big impact on obtained results and needs to be considered in AE analysis.

### 4.2 Damage mechanisms in CFRP

Understanding the different damage mechanisms that occur during increased stress conditions is vital to the damage assessment and decision-making process in a typical SHM system. In carbon fiber reinforced polymer (CFRP), debonding between the composite matrix and fibers is typically the leading mechanism, followed by matrix cracks and then, in an unspecified order, delamination and fiber breakage [13]. The nature of every mechanism is highly dependent on the situational conditions of the event, meaning that frequencies, amplitudes, energy levels, durations etc. cannot be generalized to CFRP as a whole, but must be calibrated to a specific case of material preconditions for good accuracy. [2]

#### 4.2.1 Debonding

Debonding is a local effect that separates fiber and matrix, effectively detaching the two mediums [14]. Can be seen in Figure 5 (a).

#### 4.2.2 Matrix crack

Matrix cracks are transverse fractures in the matrix. CFRP relies greatly upon the fibers for most of its valuable characteristics such as strength, and therefore, the laminates have significantly reduced qualities in the transverse direction to the fibers which can lead to matrix cracking during load. Matrix cracks are not in itself a direct point of failure but will negatively impact the mechanical properties of the material. [13] Can be seen in Figure 5 (b).

#### 4.2.3 Delamination

Delamination is the damage that occurs between plies and detaches the plies. This event is considered a much more serious damage than preceding mechanisms and can accelerate the weakening of the material. [13] Can be seen in Figure 5 (c).

#### 4.2.4 Fiber breakage

Fiber break is the damage separating fibers in two. This damage is fatal and will eventually cause failure in the composite. [13] Can be seen in Figure 5 (d).

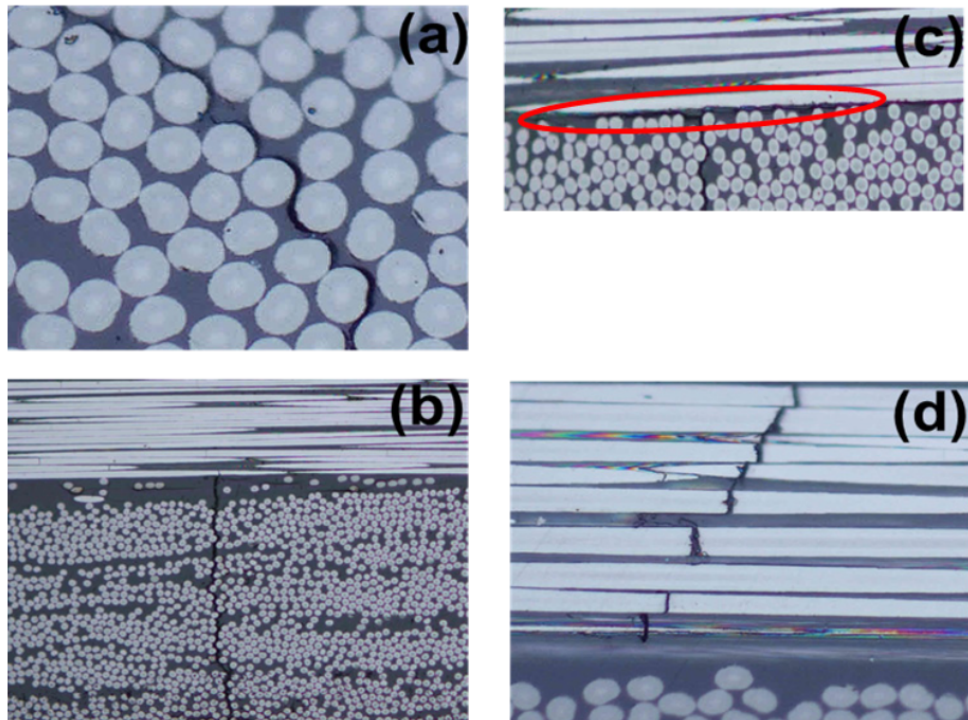


Figure 5: (a) Debonding. (b) Matrix crack. (c) Delamination between  $0^\circ$  and  $90^\circ$  layers. (d) Fiber breakage. [13]

### 4.3 Peak frequency signals from matrix cracks

As mentioned earlier, several different damage mechanisms can occur in a composite. Since debonding, matrix cracks, delamination and fiber breaks all produce AE signals, it's desirable that the AE method can determine what type of damage that has occurred [2]. Peak frequency is a popular feature to use when connecting type of damage to AE signals, where an advantage is the relative low impact of energy attenuation on peak frequency [2]. This feature does however have the drawback of being affected by resonance frequencies in the used sensor [7].

The topic of what frequency content to expect from matrix cracks has been widely reported about. In Saeedifar and Zarouchas [2] review, the authors concluded that most literature found that matrix cracks generate the lowest peak frequency compared to other damage types. Oz *et al.* [15] claims that the notion that matrix cracks generate low peak frequency signals is conventional in the literature. This might not always be the case since several studies have doubted that matrix cracks only generate low frequency signals and claim that where (with respect to the direction along the thickness) the matrix crack occur

influences the obtained frequency [12], [15], [16]. Oz *et al.* [15] measured high frequency signals caused by matrix cracks in inner 90° plies. Baker *et al.* [16] and Hamam *et al.* [12] found from their experiments that matrix cracks in inner 90° plies generate higher frequency signals compared to matrix cracks in outer 90° plies. Hamam *et al.* [12] also concluded that ply thickness affects the frequency content in signals from matrix cracks in inner 90° plies. It seems that the peak frequency from matrix cracks, relative to other damage types, might vary for different cases. Figure 6 displays the difference between inner and outer 90° plies.

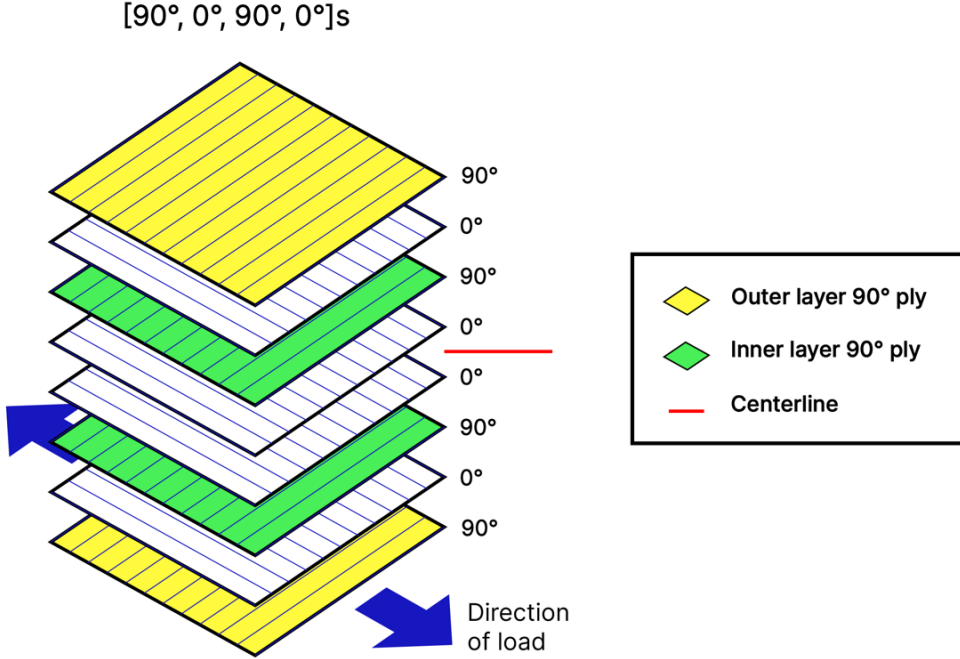


Figure 6: Displays difference between inner and outer 90° plies.

#### 4.4 Linear correlation between matrix crack density and cumulative AE energy

Matrix crack density is the number of matrix cracks per length unit. Li *et al.* [17] made tensile tests on CFRP specimens with a layup of  $[0^\circ_2, 90^\circ_4]_S$ . They found a linear model that described matrix crack density in the 90° ply as a function of cumulative energy from low peak frequency signals. However, different loading rates in the tensile tests gave different linear relations according to the study. Also, the authors found that the low peak frequency signals contained more cumulative energy than the rest of the signals. Baker *et al.* [16] used CFRP specimens with  $[90^\circ, 0^\circ]_{6S}$  layup for tensile testing. They found that the cumulative energy from low peak frequency signals was linearly correlated with the matrix crack density in the outer 90° plies. Linearity was also shown between the cumulative energy from high peak frequency signals and the matrix crack density in the interior 90° plies.

#### 4.5 Damage localization techniques

AE methods can be implemented to locate damage through assuming constant wave propagation velocity through the medium and knowing the distance between two or more sensors [18]. However, the anisotropic nature of composites results in the waves propagating at different velocities in different directions, which makes it significantly harder to reliably locating damage in composites using AE [19]. More complex methods to increase the accuracy of locating damage have been proposed by Ciampa and Meo [19] and Al-Jumaili *et al.* [20].

## 5 Experimental methodology

Experiments are a necessity in scientifically evaluating the AE method. Without experiments there would be no tangible way to confirm the accuracy of the tools developed in this study. In motivating which tests to conduct, many aspects of the examined theory will lay as the groundwork. This chapter is designated to the methodology of our experiments.

### 5.1 Tensile machine

The machine used for conducting tensile tests on the CFRP specimen in this project is the Instron 5582 Universal Tester, or “Fat Tony”, provided by the construction material laboratory at Linköping University.

### 5.2 Acoustic emission sensor

As mentioned in the theory chapter 4.1.3, a sensor used to collect signal waveforms from acoustic emissions needs to be specifically tuned for this purpose. MINI30S is a small piezoelectric AE sensor developed by MISTRAS that fits the specifications and was used for testing in this project. The sensor has an operating frequency range of 270 - 970 kHz and a resonant frequency of 325 kHz. However, the last time the sensor was calibrated was over 20 years ago, when the sensor was manufactured. Calibrating the sensor was not an option because of budgetary restraints.

### 5.3 Acquisition setup

A USB AE Node is used, developed by MISTRAS group, to acquire signals from the sensor. The system is connected to a computer where the belonging software program AEwin computes hits and extracts features using a threshold in the same way as explained in chapter 4.2.2. Table 2 shows the important settings chosen in AEwin for all measurements made.

*Table 2: Chosen settings in acquisition setup*

Threshold	Lower analog filter	Upper analog filter	Sample rate	PDT	HDT	HLT
45 dB	20 kHz	1 MHz	5 MHz	35 $\mu$ s	150 $\mu$ s	300 $\mu$ s

The timing parameters PDT, HDT and HLT are chosen based on the recommendation from the USB AE Node manual [6]. These recommendations are displayed in chapter 4.2.2. The threshold is set relatively

high to avoid background noise. Figure 7 displays the acquisition setup including the USB AE Node, a computer, and the connector to measure load from the tensile machine.

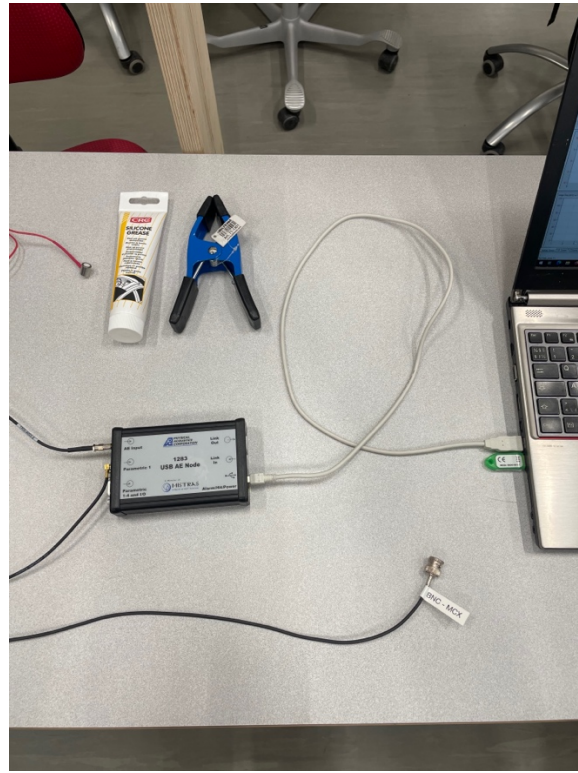


Figure 7: The acquisition setup. The USB AE Node is connected to a computer, where data is computed and stored. The connector seen at the bottom of the picture is connected to the tensile machine to measure the load.

#### 5.4 CFRP testing specimen

Specimens are provided by Berggren *et al.* [21]. How these specimens are manufactured can be read about in their study. The specimens are made of UD prepreg with the layup  $[0^\circ, 90^\circ, 0^\circ, 90^\circ]_S$  with ply thickness of about 145  $\mu\text{m}$ . Figure 8 displays the layup sequence.

A layup with outer 90° plies is avoided. Because matrix cracks in outer 90° plies might mainly produce low frequency signals [12], [16] as discussed in chapter 4.3, this could have been a problem since our sensor has poor sensitivity below 270 kHz. Only one layup is used since it is expected to be variations in the damage accumulation and AE signals with different layups. The use of only one layup makes it easier to compare the results.

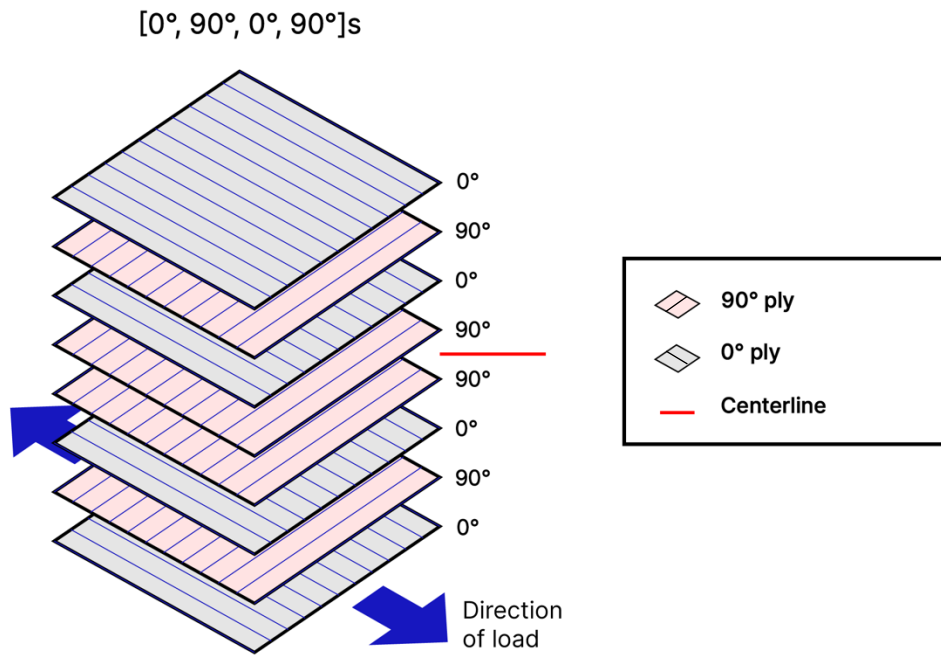


Figure 8: Displays the layup on the specimens used in the experiments.

Some of the specimens had end tabs attached and Tabrizi *et al.* [22] claims end tabs are used “To assure occurrence of failure at gauge length of the specimen” [22, p.2] and “the usage of end tabs, which can transfer clamping force to the specimen through shear action, is specifically recommended for unidirectional laminates” [22, p.2]. The tabs were attached using epoxy and they are made from glass fiber reinforced polymers. Figure 9 show a specimen with tabs attached and one without tabs. Table 3 shows which specimens had tabs.

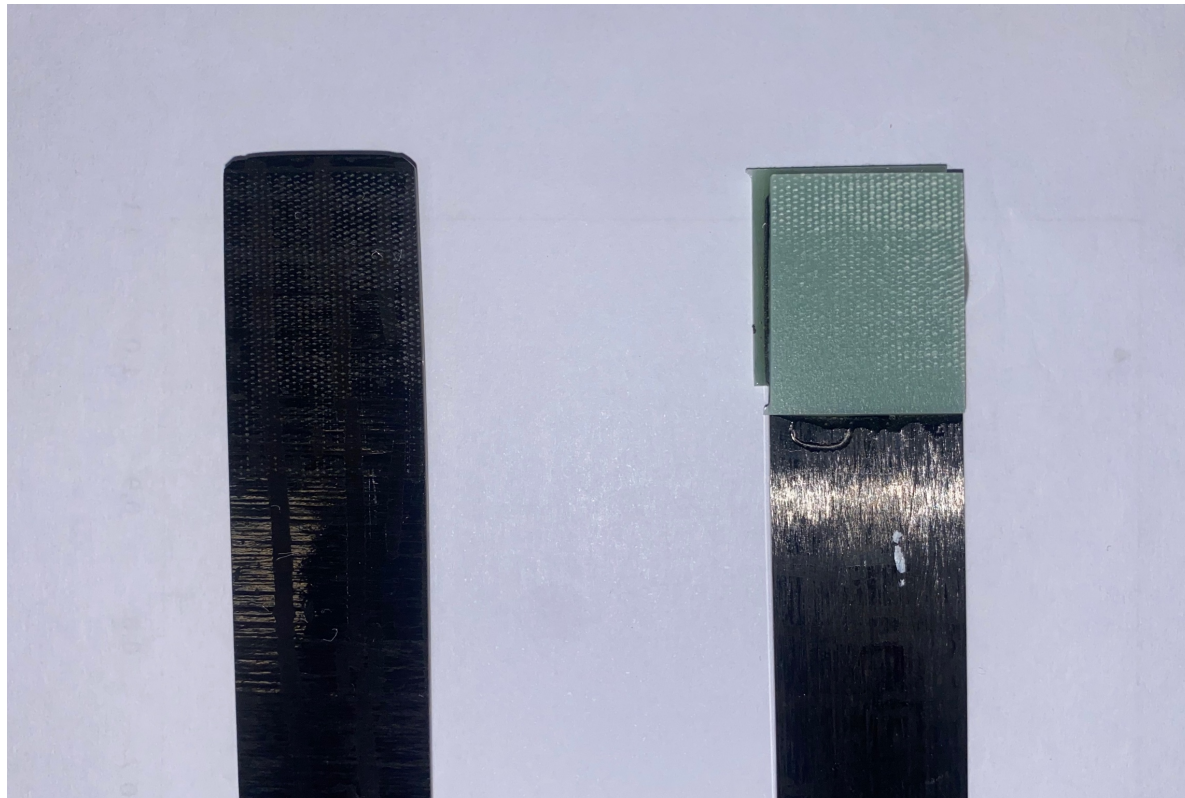


Figure 9: Specimen without tabs adhered (left) and specimen with tabs adhered (right).

The gauge length can be difficult to determine on specimens without tabs since the gripping from the tensile machine and the specimen can be uneven. Figure 10 shows a specimen without tabs after a tensile test where you can see that the real gauge length and the measured gauge length can differ. The indentations from the tensile machine grips are gradually more prominent further down the specimen. Which indicates that the real gauge length is somewhere in between the measured gauge length and the end of the specimen without tabs. Therefore, the strain cannot accurately be calculated.

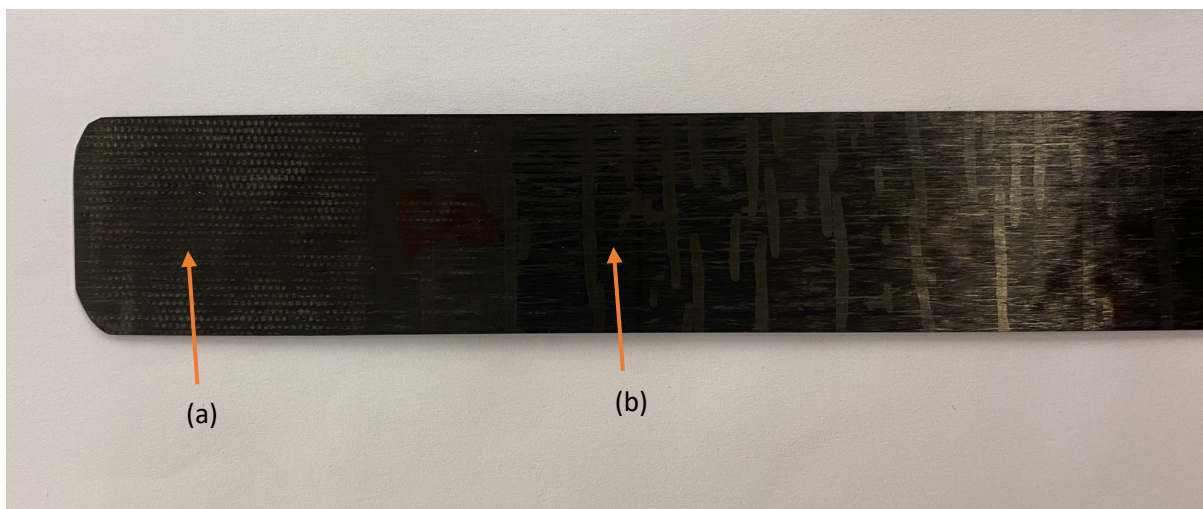


Figure 10: Specimen with indentation from tensile machine (a) and line that show where gauge length start was measured when mounted (b).

## 5.5 Experimental setup

First, the specimen is fixed in the tensile machine. Then the sensor is clamped on the middle of the specimen and held fixed with a glue clip. Silicone grease is placed between the sensor and specimen to increase acoustic contact, as discussed in 4.2.4. The USB AE Node is connected to the tensile machine and measures the load from the tensile machine. This allows the data from the sensor to be compared with the tensile stress on the specimen. The experiments were performed together with Berggren *et al.* [21]. They handled the setup of the specimen in the tensile machine and the tensile test, while the authors of this study handled the acoustic emission acquisition measurement and setup. Berggren *et al.* [21] also provided the strain data from the experiments.



Figure 11: Experimental setup. The specimen is mounted in the tensile machine and the sensor is held fixed onto the specimen with a clamp.

## 5.6 Hsu-Nielsen source testing

Before each test, a 2H 0.5mm lead with length of about 3mm is broken 5-6 cm away from the sensor. It's required that the sensor should record an amplitude between 95-100dB, where 100dB is the maximum amplitude the system can record, to ensure proper coupling and repeatability between the tests.

## 5.7 Testing

Tensile tests are made on each specimen with a loading rate of 2mm/min until the maximum tensile stress is reached. After the maximum stress is reached the load is held constant, and the AE measurement is canceled when the curve for cumulative energy flattens out. At most ten seconds after the AE measurement is finished, the tensile machine stops applying load to the specimen. For every test, a new specimen is used. The maximum load for each test differs between 200-700 MPa (~ 0,36 - 1,6 % strain). Table 3 shows the maximum stress for each test made.

*Table 3: Maximum tensile stress for each test, dimensions of the specimens and if the specimen had end tabs. Dimension data is provided by Berggren et al. [21].*

Test number	Maximum stress (MPa)	Dimensions (mm) Length x Width x thickness	End tabs
1	200	132 x 21,9 x 1,15	No
2	200	142 x 19,3 x 1,15	No
3	250	147 x 20,5 x 1,15	Yes
4	250	148 x 21,8 x 1,15	Yes
5	300	146 x 21,7 x 1,15	No
6	300	146 x 21,7 x 1,15	Yes
7	350	148 x 22,1 x 1,15	Yes
8	350	154 x 22,5 x 1,15	Yes
9	400	132 x 19,9 x 1,15	No
10	500	143 x 22,5 x 1,15	No
11	550	144 x 22,3 x 1,15	No
12	600	140 x 18,8 x 1,15	No
13	650	147 x 22,3 x 1,15	No
14	700	129 x 21,6 x 1,15	No

### 5.7.1 Incremental load increase

One way of verifying the theory that matrix crack density is correlated to cumulative energy, as discussed in chapter 4.4, is by conducting tensile tests with multiple specimens and incrementally increase the max load of each test. This way one can optically verify the amount of matrix cracks at each stress level and compare this to the observed cumulative energy levels. If a correlation is confirmed, this can potentially be used as an indicator in parallel with other damage identification methods. In addition to the aforementioned purpose of an incremental load increase experiment, one can also analyze every tests independently to verify other aspects and characteristics of the damage mechanisms without resorting to conducting new tests. It is important that the tests in this method are designed with identical timing parameters and software parameters to get un-biased results.

## 5.8 Detecting matrix cracks using microscope

Berggren *et al.* [21] used an optical microscope to look for matrix cracks in each specimen after tensile tests. How this was done can be read in their report. In short summary, both sides of each specimen were polished before tensile tests were made. Matrix cracks are counted on both sides of each specimen, and an average of matrix cracks is computed as the number of counted matrix cracks on both sides divided by

two. Cracks were only counted between the glass fiber tabs. No counting was made on specimens without tabs, except for specimens 1 and 2 where the whole length of the specimen was considered. This was done to see if any matrix cracks occur at this stress level.

## 5.9 Data analysis

After the data accumulation process has been handled in the AEwin software, hits with their features, waveforms and some output variables calculated in AEwin are exported to MATLAB via .TXT or .CSV files, where signal processing and analysis is conducted. Each waveform is loaded in and passes through several filters to sort out relevant signals. For each hit, about 1.4 ms of the hits waveform is saved. First, a waveform's length is compared to the perceived duration of the hit. If the duration is longer than the data collection time parameter, it can be concluded that some data might be lost in the process. This might affect the calculation of peak frequency. Generally, every data set will always contain hits which durations exceed the collection time unless the collection time is set extremely high. The drawback to doing this is simply that it takes up a lot of hard drive storage and will take longer for the software to process since it essentially multiplies the amount of information in every file. Since AEwin collects every waveform in its separate text file the number of files can often be upwards of thousands.

### 5.9.1 Damage mechanism definition

The purpose of the MATLAB script is to automate most of the analyzing and would in an ideal world simply output the number of matrix cracks solely through waveform input. However, to get more accurate results and to free up memory, the MATLAB script relies upon some calculations that are done by AEwin, which include (see chapter 4.1.2 for feature definitions):

- Time of hit
- Amplitude
- Counts to peak
- Counts
- Risetime
- Absolute energy
- Duration

Other calculations that are not supported by AEwin and must be done by the MATLAB script include:

- Peak frequency

Some data output from the tensile machine can also be channeled through the parametric input of the AE node, such that another feature can be recorded. This feature is referred to as parametric data and outputs load data.

## 6 Results & Analysis

This chapter displays the results of the experiments and the analysis of these results.

### 6.1 Cumulative hits vs tensile stress

Figure 12 shows the cumulative hits against applied stress for all tests conducted. It can be seen that small amounts of hits occur at low stress levels under 200 MPa ( $\sim 0,36\%$  strain). Some of these hits are likely caused by noise such as friction between the specimen and tensile machine grips. No matrix cracks were found for the two specimens with maximum stress of 200 MPa which makes it unlikely that any matrix cracks occur below this stress level, but it's still possible. Other types of damage could also occur at low stress levels and cause these hits. At around 200 - 250 MPa, the slope for cumulative hits increases. It seems that during this period, damage accumulation in the specimen starts accelerating. After this period, the slope seems to stay linear for all the tests until the maximum stress is reached.

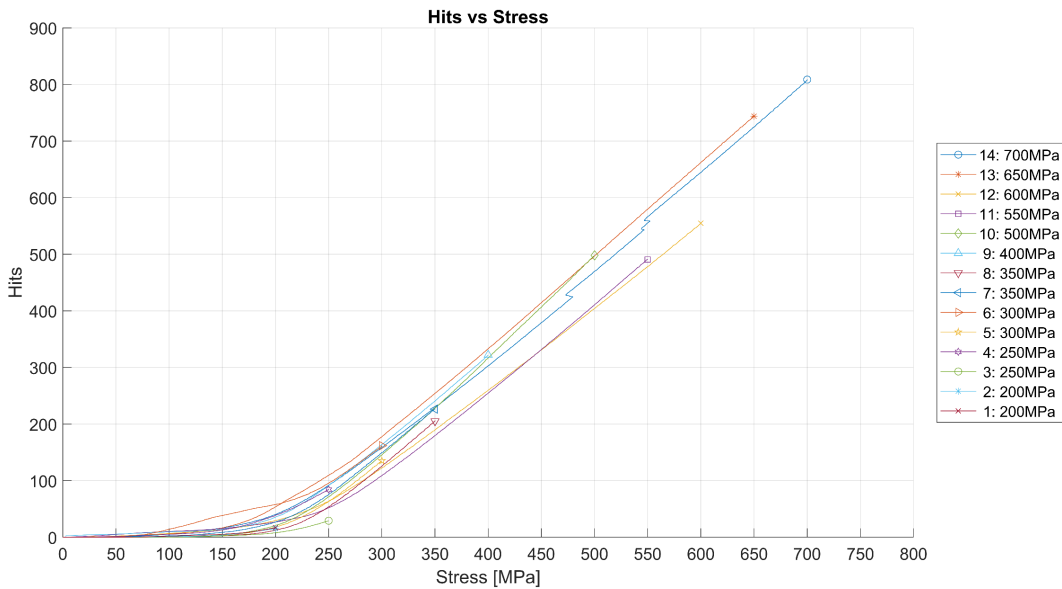


Figure 12: Cumulative hits vs stress for all tests made. Legend: tests 1 – 14, total stress accumulation.

After the maximum stress is reached, the stress is held constant for some time. The time where the maximum stress is reached is referred to as pullstop. Figure 13 shows the percentage of the total cumulative hits against time after pullstop for all tests. In general, the curves flatten out which indicates that damage accumulation slows down with time after pullstop.

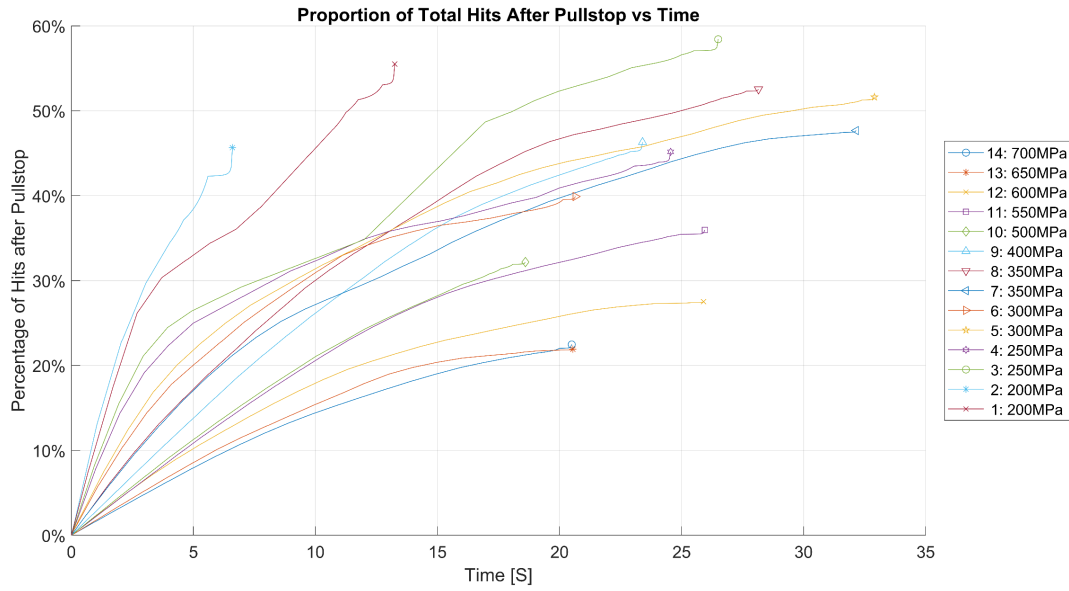


Figure 13: Percentage of cumulative hits against time after pullstop. Legend: tests 1 – 14, total stress accumulation.

## 6.2 Cumulative energy vs stress

Figure 14 shows the cumulative energy for all tests plotted against stress. In contrast to the curve for cumulative hits against stress, the cumulative energy seems very sporadic and heavily influenced by single hits with large energy. Variations are possible due to quality variations in the specimens creating variance in the damage accumulation process. Noise could also cause hits with considerable energy. The large spikes in energy for single hits could be caused by matrix cracks, but they could originate from some other damage type. Since only matrix cracks are looked for in the optical microscope, we can't know what other types of damage that occurred in the specimens. If the assumption is made that these high energy hits are not mainly caused by matrix cracking, but instead some other type of damage, and remove these from the plot interesting results occur as seen in Figure 15. Here all hits with an energy above  $1.5 * 10^7 \text{ aJ}$  are filtered out. Now a more general pattern can be observed. Most tests show a significant increase in energy at around 220 - 230 MPa, which equates to about 0,42 - 0,45 % strain in accordance with our test results.

Looking at Figure 16, it shows that the energy increase holds until about 400 MPa, after which the energy released is lessened.

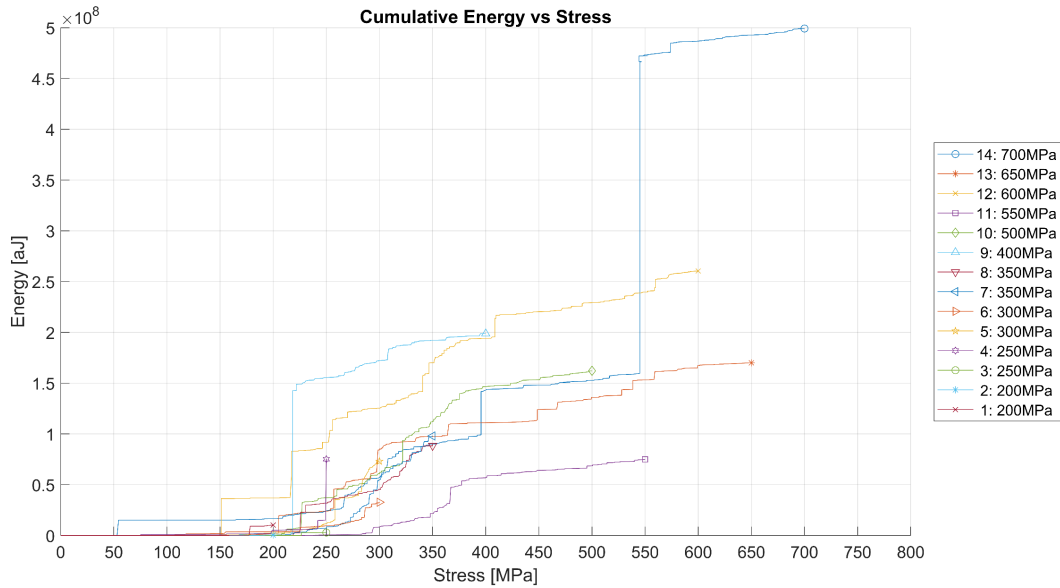


Figure 14: Cumulative energy vs stress for all tests. Legend: tests 1 – 14, total stress accumulation.

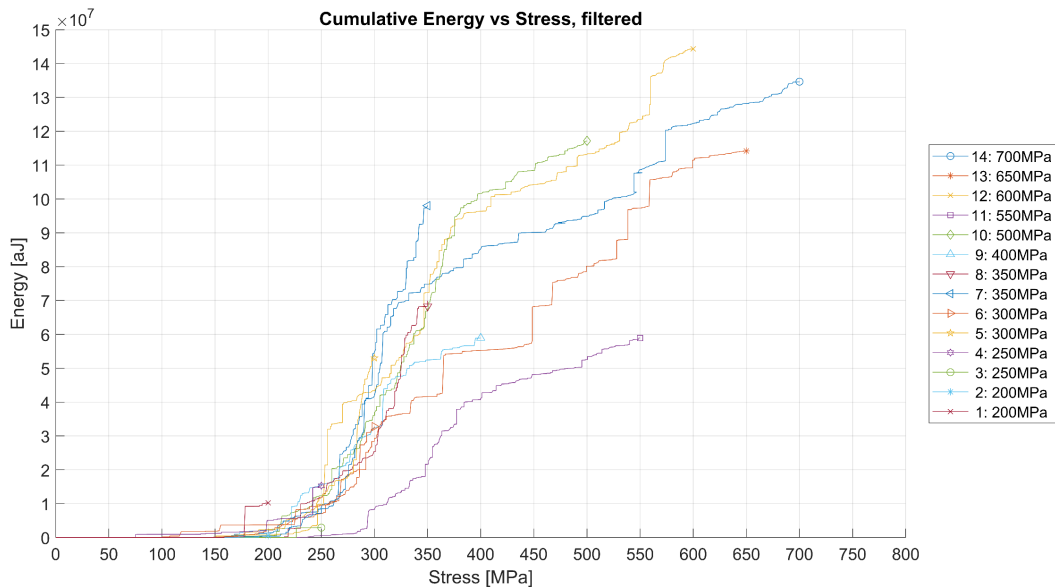


Figure 15: Cumulative hits vs stress for all tests after filtering out hits with higher energy than  $1.5 \times 10^7$  aJ. Legend: tests 1 – 14, total stress accumulation.

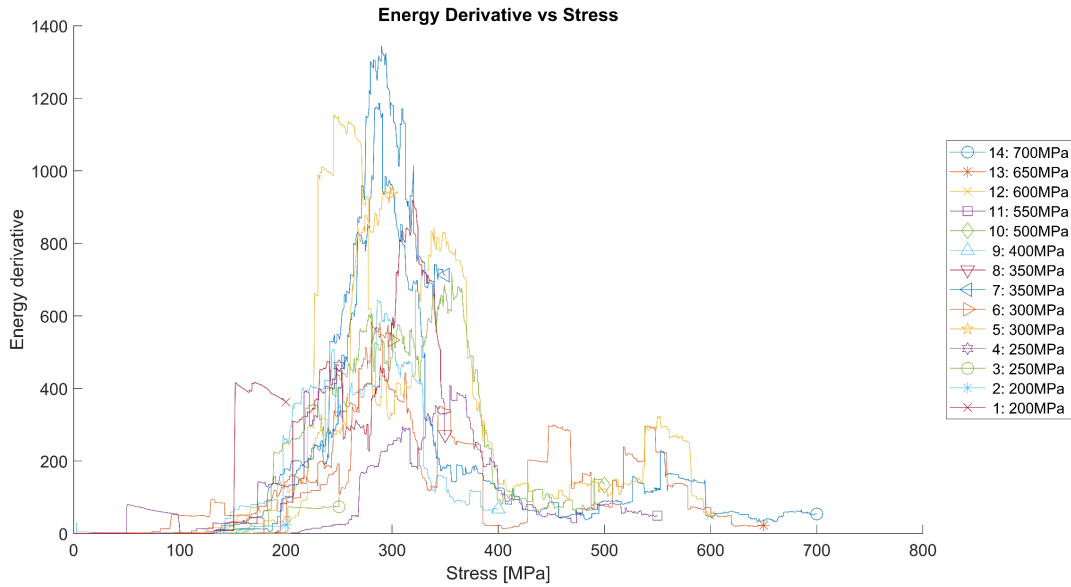


Figure 16: Energy derivative vs stress. Legend: tests 1 – 14, total stress accumulation. tests 1 – 14, total stress accumulation.

The cumulative energy after pullstop is seen in Figure 17. It can be seen that a significant portion of energy comes after pullstop, especially for specimens pulled below 400 MPa ( $\sim 0.80$  % strain). The rise in cumulative energy followed by being flattened after pullstop indicate that damage accumulation after pullstop slows down with time. The same pattern is seen in Figure 18 where the high energy filter is applied, the difference being that a higher percentage of energy comes after pullstop for some tests since the total cumulative energy was reduced by the filter.

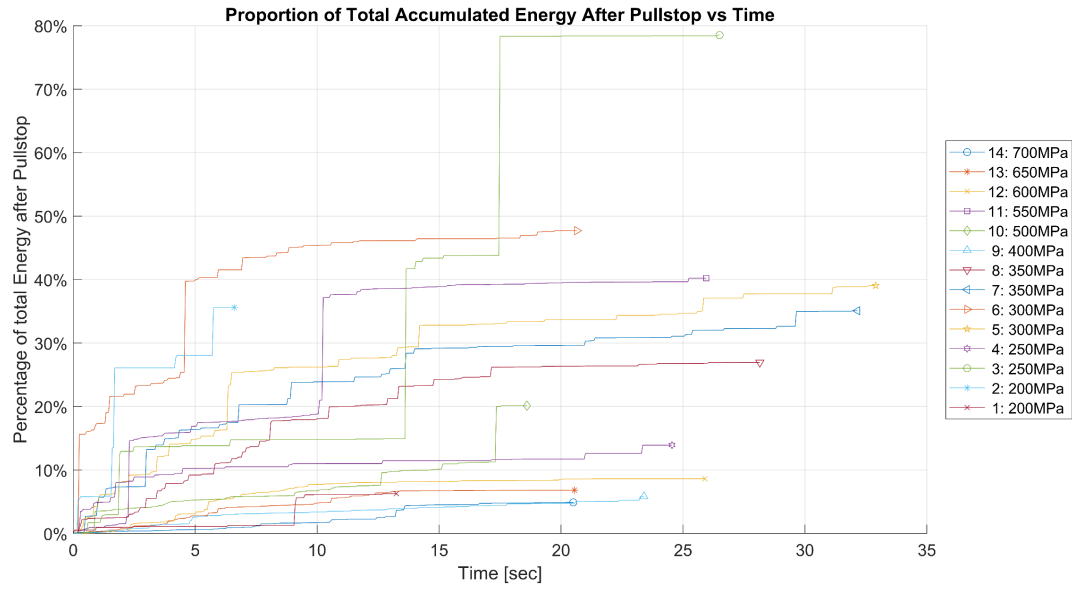


Figure 17: Percentage of cumulative energy against time after pullstop. Legend: tests 1 – 14, total stress accumulation.

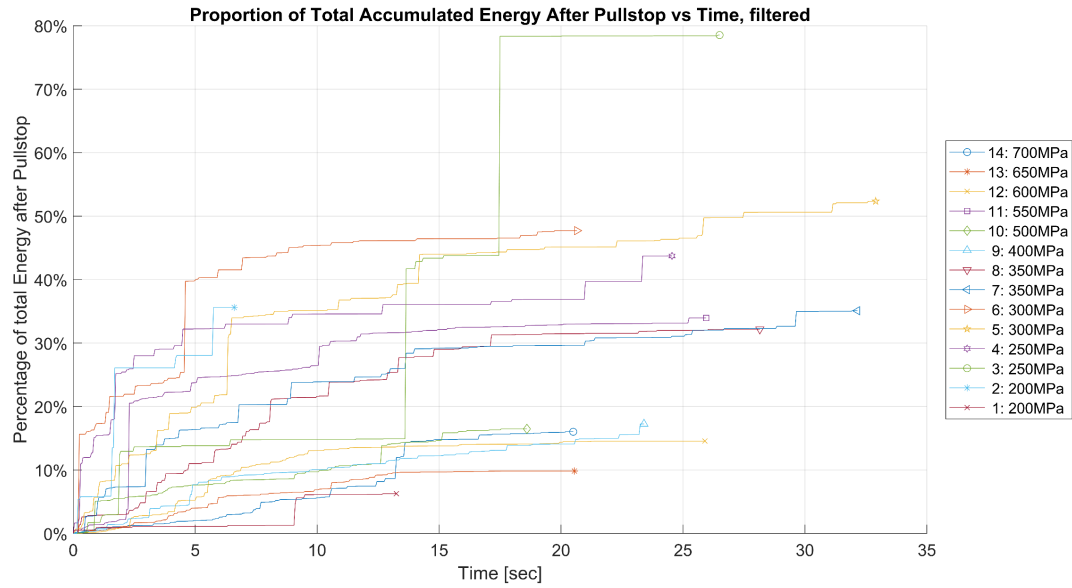


Figure 18: Percentage of cumulative energy against time after pullstop after filtering out hits with higher energy than  $1.5 \times 10^7$  aJ. Legend: tests 1 – 14, total stress accumulation.

### 6.3 Peak frequency results

As mentioned earlier, only about 1.4 ms of a waveform are saved for every hit. These waveforms are used when calculating the peak frequency of each hit using FFT. Miscalculations occur when the duration of the hit exceeds 1.4 ms because the whole waveform is not included in the computation of the peak frequency. As shown in the figure below, most hits do not have a duration that exceeds the collection time. In this example, about 14 hits out of 955 had too long duration to accurately calculate frequency features.

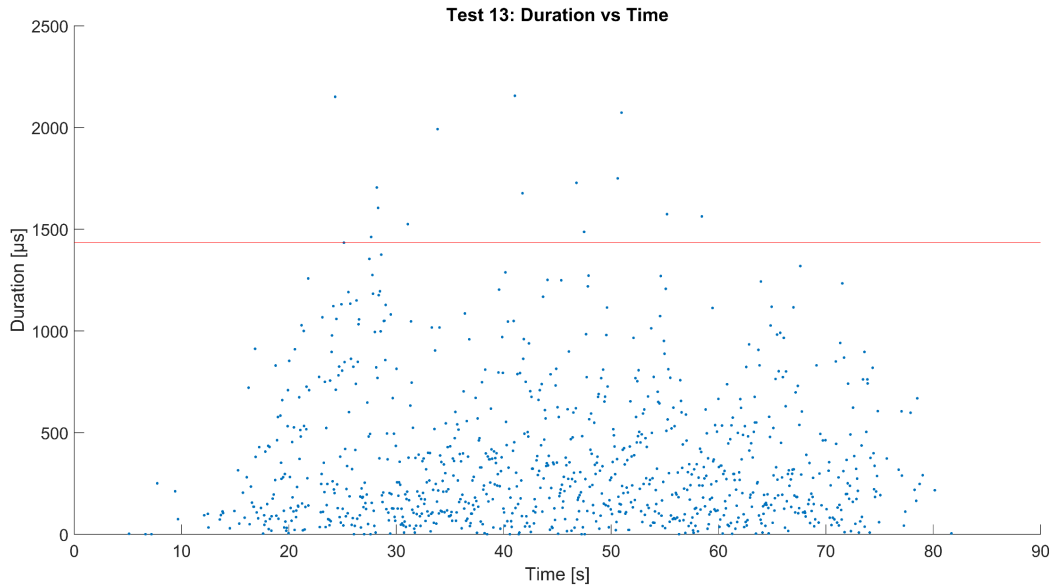


Figure 19: Duration vs time of test 13 as an example. Collection time indicated by red line.

The frequency contents of all tests remain similar in all cases, as illustrated in the figure below. Peak frequency is consistently spiking around 28 - 43 kHz, 79 - 94 kHz, 298 - 328 kHz, and 517 - 560 kHz. The 298 - 328 kHz range stands as the highest hit count among all frequencies and is likely due to the sensor causing an over-representation of frequencies around its resonant frequency of 325 kHz. The lower frequencies (< 270 kHz, which is the lower operating frequency limit), however, are unexpected in the sense that the frequency sensitivity of the sensor is very low in that frequency band. This is probably the result of an over-amplification of certain frequencies, or some kind of error in peak frequency calculation, which would indicate that the true peak frequency lies elsewhere.

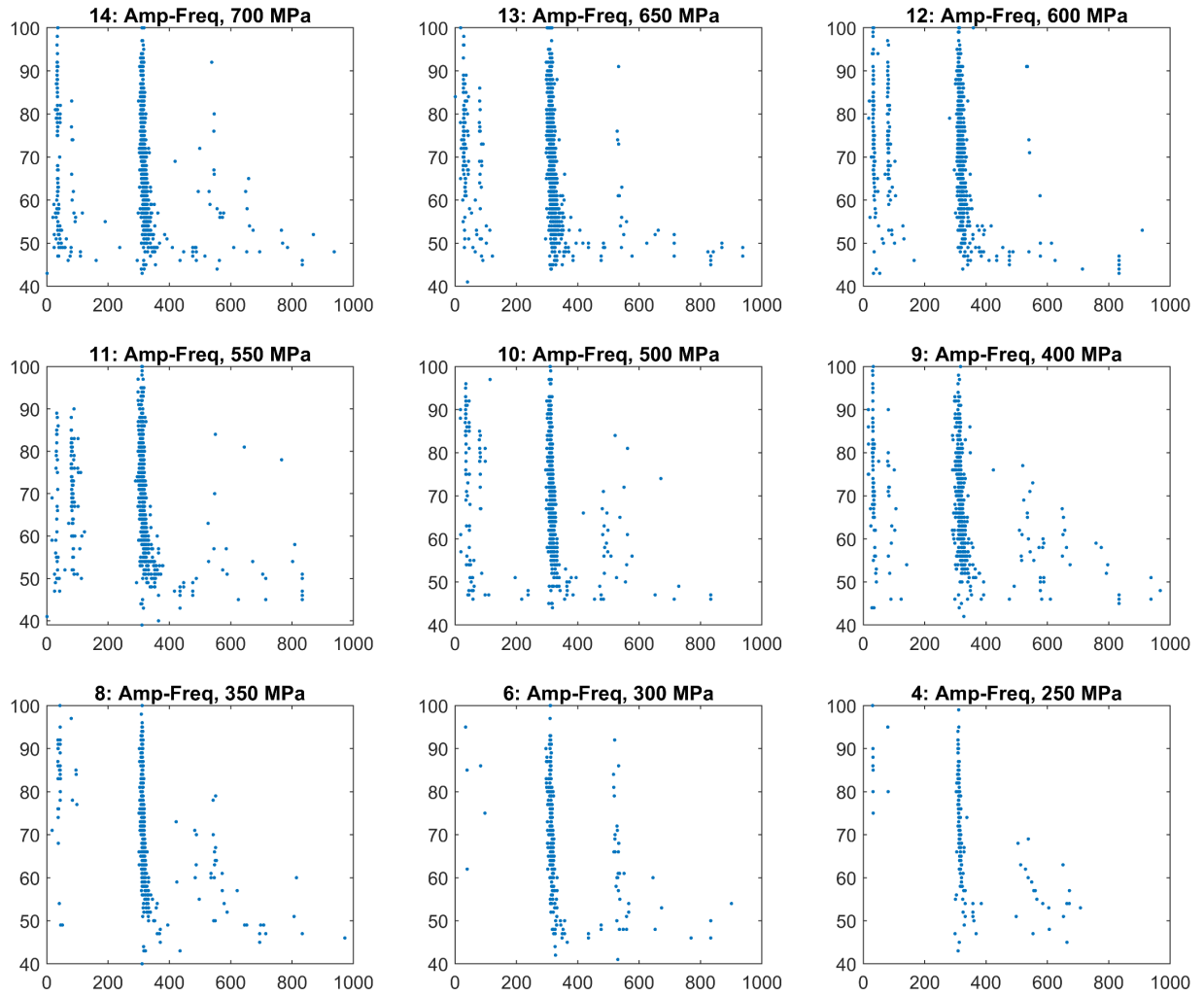


Figure 20: Amplitude (y, dB) vs peak frequency (x, kHz). Each dot indicates one hit. Some tests with duplicate maximum stress were excluded.

#### 6.4 Matrix crack data

Table 4 shows the average number of matrix cracks for the specimens with tabs, and specimen 1 and 2. For these specimens, there were only matrix cracks found in the double 90° ply. Tests 6 and 9-14 were not analyzed for matrix cracks.

Table 4: Test number, max stress, and matrix crack data. Matrix crack data provided by Berggren et al [21]

Test number	Max Stress	Matrix Cracks side 1	Matrix Cracks side 2	Matrix Cracks Propagated	Average number of cracks per side
1	200	0	0	0	0
2	200	0	0	0	0
3	250	3	5	3	4
4	250	5	2	1	3,5
5	300	28	29	13	28,5
7	350	95	118	87	106,5
8	350	80	121	79	100,5

## 6.5 Cumulative energy to describe amount of matrix cracks

As discussed in chapter 4.4, linearity has been found in previous studies between matrix crack density and cumulative energy [16], [17]. However, these studies also used the peak frequency to distinguish which signals are related to matrix cracks in the ply of interest. Since the peak frequency from our experiments are not considered sufficiently reliable, as discussed in chapter 6.3, we will not use this feature to sort signals. Since we only have verified the number of matrix cracks for seven specimens, we can only use the AE data from these tests.

What cumulative energy to choose must also be decided. As shown in chapter 6.2, a filter which removes high energy signals could be used. This filter assumes that high energy hits primarily contain energy from other sources than matrix cracks, but there is no way of knowing whether this assumption is accurate or not. The accuracy also depends on chosen energy level for the filter. In our case it's  $1.5 * 10^7 \text{ aJ}$  and choosing a different level will change the results. Therefore, this filter should be considered as an unproven alternative to filtering using peak frequency.

As shown in chapter 6.2, a considerable portion of cumulative energy is obtained after pullstop. The cumulative energy from pullstop or from end of the AE test could be used. Whichever is more accurate depends on, after pullstop, how many new matrix cracks that occur and how big the portion of energy that originates from new matrix cracks is compared to other damage types and noise. Both these factors are unknown.

Two choices could be made regarding the cumulative energy, creating four combinations. These four combinations of cumulative energy are plotted against the average number of matrix cracks verified using an optical microscope, and is shown in Figure 21, Figure 22, Figure 23, and Figure 24. A linear regression curve is also computed.

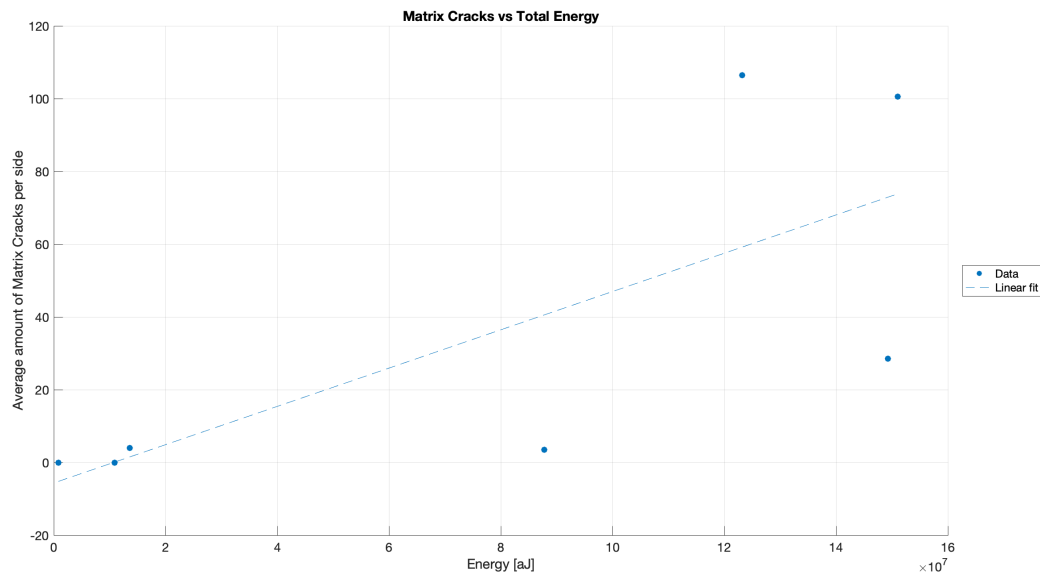


Figure 21: Amount of Matrix cracks observed optically under microscope vs amount of total energy recorded with AE setup.

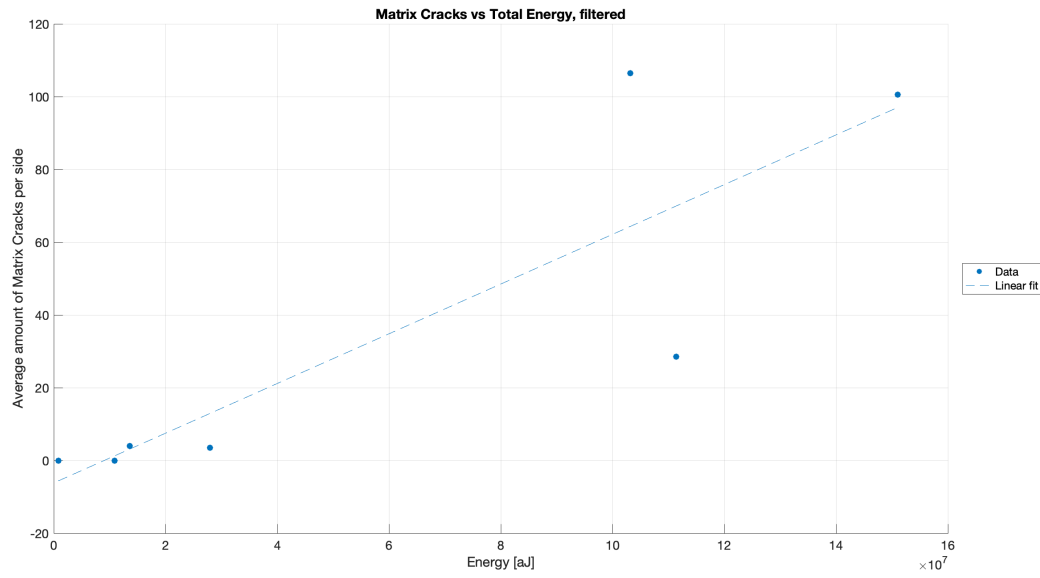


Figure 22: Amount of Matrix cracks observed optically under microscope vs amount of total energy recorded with AE setup. High energy events are filtered out.

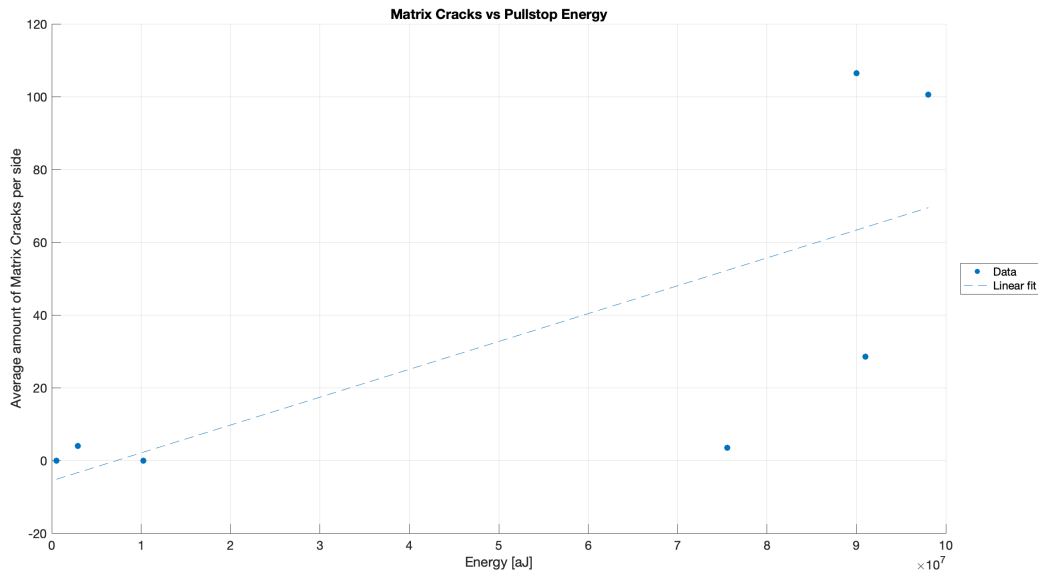


Figure 23: Amount of Matrix cracks observed optically under microscope vs amount of energy recorded up until pullstop with AE setup.

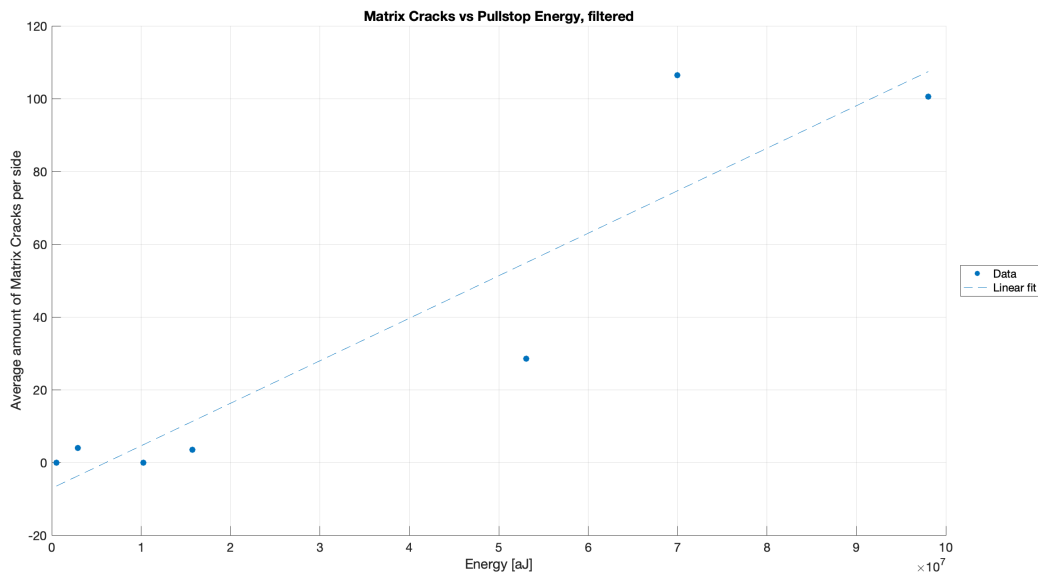


Figure 24: Amount of Matrix cracks observed optically under microscope vs amount of energy recorded up until pullstop with AE setup. High energy events are filtered out.

Since there are only seven data points, observations are only indications and not conclusions. All plots indicate that there might exist a linear relation, where Figure 24 has the best linear fit for the data points. However, with more data any of these plots could prove to be most accurate in predicting the number of matrix cracks. At the same time more data could show that a linear model is too inaccurate. Again, more data is required to clarify the reliability of these proposed linear models.

## 6.6 Example of implementation of cumulative energy to predict cracks vs stress

One method of using cumulative energy to predict the number of cracks on a specimen after it has been loaded to a specific stress can be calculated with regression. In this example we have seven points where the maximum stress and the accumulated acoustic energy has been measured and on two of those specimens the number of cracks is known. If we draw a line between those points, we get a function describing the expected number of cracks for a specific accumulated acoustic energy. The two chosen specimens and the line can be seen in Figure 25. The figure also shows that this model is not very accurate since the other data points are not very close to the line. Also note that the chosen example has the most linear behavior of the results in 6.5. The data has been filtered and the accumulated energy is at pullstop.

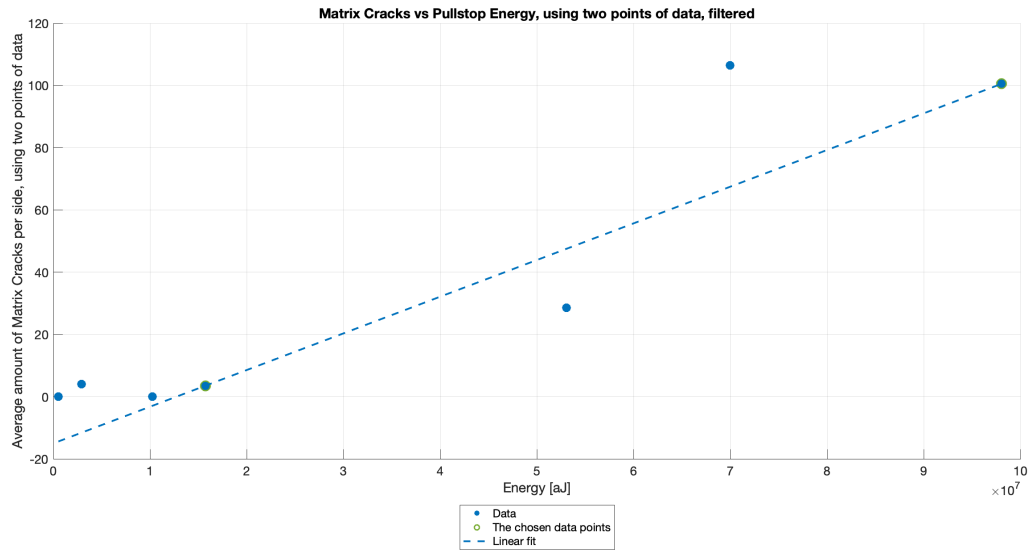


Figure 25: Average number of matrix cracks per side of the specimen vs the accumulated energy at pullstop.

Then the accumulated acoustic energy is then plotted against the max stress and a polynomial regression fit is calculated with the points. We chose a second-degree polynomial since it gave a sufficient fit. The point and the fit can be seen in Figure 26.

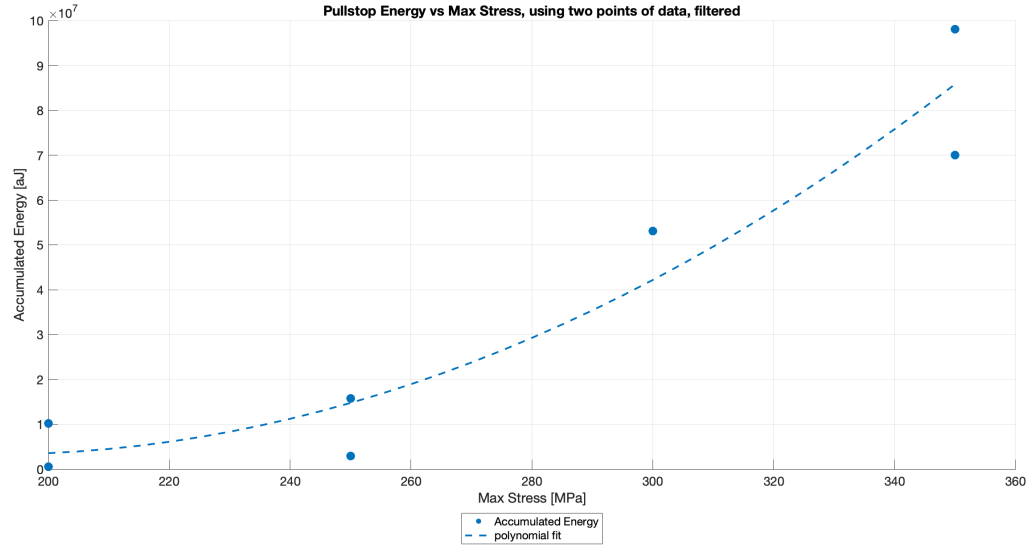


Figure 26: Accumulated acoustic energy vs max stress. With a second-degree polynomial fit.

With the linear function given from the line between the two points of matrix cracks vs acoustic energy and the second-degree polynomial derived from the acoustic energy vs max stress points the expected number of cracks for a given stress can be calculated. The function derived can be seen plotted in Figure 27 alongside the real data where the matrix cracks has been counted optically.

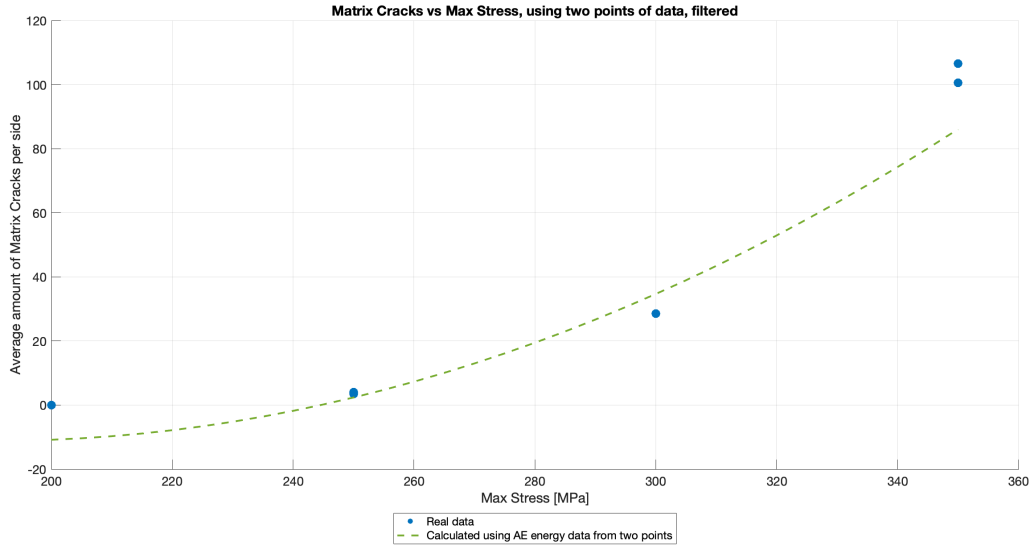


Figure 27: Average number of matrix cracks per side vs max stress. Points with optically counted cracks and the calculated function of the expected number of cracks.

The function given shows that a model to describe the expected number of cracks in a specimen can be predicted using limited crack count data. The purpose of this example was to show how you can make a layup specific model to predict matrix cracks in a specimen by only counting the cracks in two specimens that have been subjected to two different stresses. This model assumes that acoustic cumulative energy and matrix cracks have a linear relationship in the stress test span, which we have not investigated for other layups nor can prove for our layups since there isn't enough data. Theoretically, this model can yield similar results if strain is used instead of stress.

If two other point in the same dataset is chosen the function will look different but attain a similar behavior. Figure 28 shows the function derived from two other points. The change gives a difference of about 50 matrix cracks per side at 350 MPa, which is a quite substantial change.

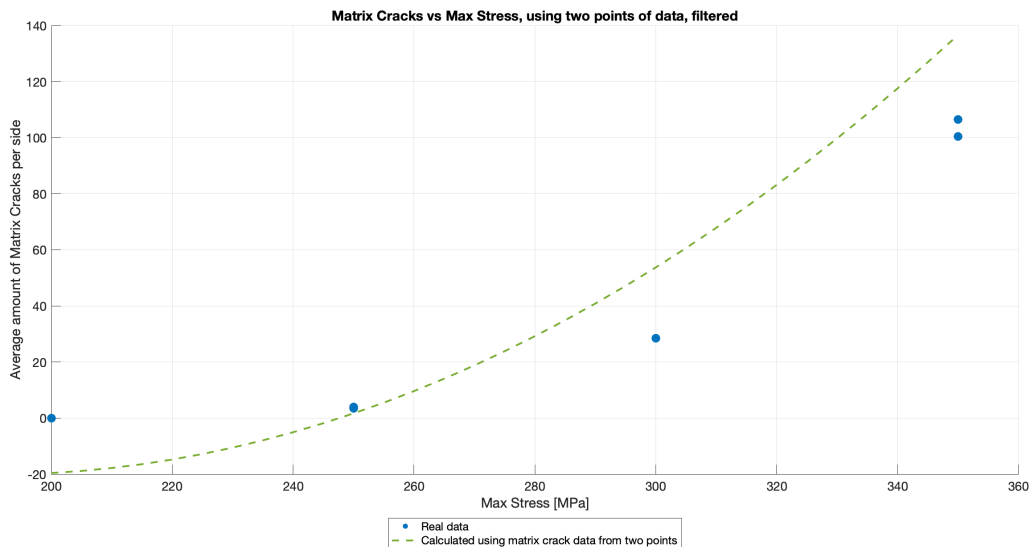


Figure 28: Average number of matrix cracks per side vs max stress. Points with optically counted cracks and the calculated function of the expected number of cracks. With two other points.

## 7 Discussion

In this chapter, the reliability of the results is discussed and how these results relate to previous studies. Improvements for future studies are also proposed.

### 7.1 Automating filter algorithms

Some of the processes developed in this study are not automated and could likely be implemented such that no human intervention is needed in investigating the amount of matrix cracks present. One way of circumventing some aspects of the manual process would be to develop standardized cases for different layups and conditions.

### 7.2 Why multiple sensors might be necessary

One of the major challenges in the field of AE-based SHM systems is around the seemingly impactful phenomena that the energy, amplitude, and frequency of a waveform attenuates over a distance. Because of this, the larger the object, the larger the disparity will be between measured features and real features. By tuning the frequencies, amplitude, and energy levels to different distances to the sensor one could potentially collect any AE across any distance and output the same, predictable characteristics. However, there is no real way of verifying this hypothesis by the way experiments were performed in this report. The requirements for this to be possible would require a locationally controlled induction of stress, which could be done by weakening the specimen around a certain distance from the sensor, for example by reducing the cross-sectional area locally. On the other hand, this would likely alter the characteristics of the damage mechanisms, which would prove difficult to analyze without a clear model for different cases of material preconditions. Alternatively, one could employ a different method altogether, such as using the Hsu-Nielsen source method to controllably induce AE at variable distances and use those signals to tune the processing software accordingly.

At this point it is hard to tell exactly how the implementation of multiple sensors would work. As mentioned in chapter 4.5 composites are anisotropic and that sound waves propagate inconsistently in different directions [19]. This might hinder the pursuit of eliminating the negative effects of energy attenuation. As also mentioned in chapter 4.5, more accurate methods for locating damage, involving complicated techniques, exists [19], [20]. However, these methods are beyond the scope of this thesis.

Nevertheless, it is fair to say some applications naturally need multiple sensors to achieve full coverage simply because the attenuation towards some points along the body is enough to reduce the signal strength below hardware thresholds. As the purpose of this study revolves around small-scale laboratory environment use of AE and CFRP research, it can be said that multiple sensors will not be a vital element for the effectiveness of the method, but it is certainly an object for further investigation.

### 7.3 Sources of errors

In our experiments, many sources of error are possible. The possible errors we expect are the following:

- **Specimen dimensions:** There is a variation in length and width of the used specimens which could influence the comparison of AE signal data between different tests.
- **Specimen quality:** The specimens used could vary in quality and therefore the damage accumulation is also likely to vary between specimens. Since matrix cracks is the only damage mode verified, the variation of other damage types is unknown. This becomes an error since the sensor likely obtains AE signals from other damage types.
- **Verification of matrix cracks with optical microscope:** This work was done by Berggren *et al.* [21] and not by the authors of this thesis as already mentioned in chapter 5.8. Since this work is done by manually counting matrix cracks using an optical microscope, miscalculations are possible. The quality of polishing also influences how many matrix cracks are optically observed [21].
- **Energy attenuation:** As already mentioned in chapter 4.1.6, AE signals are affected by the distance between the source of the AE event and the sensor [11]. The variations in dimensions and quality of the specimens could result in different influence from this error source.
- **Used sensor:** Since it was a long time ago since the sensor was last calibrated, the sensor might not be reliable. However, the measured amplitude from pencil lead breaks matches what is expected.
- **Sensor coupling:** A pencil lead break test was performed before each test to check the sensor coupling, but variations in coupling quality is still expected.
- **Noise:** Small variations in test preconditions may affect the amount of noise present which in turn may impact the total accumulation of energy.

### 7.4 Limitations of cumulative energy to predict number of matrix cracks

In chapter 6.5, attempts are made trying to find a linear model between the number of matrix cracks in the double 90° ply, for stress levels up to 350 MPa, and cumulative energy. As already mentioned, only seven data points are used. This is a very small sample size, which means that such a model needs more data to confirm the relation and validate the accuracy. The errors between the models and data points can partly be caused by errors discussed in chapter 7.3.

Previous studies, as mentioned in chapter 4.4, similarly used the cumulative energy for the same purpose but also filtered signals using peak frequency [16], [17]. Because of its unreliability in our experiments, we never used peak frequency, but instead applied a high-energy filter. For our tests, this filter seems to give the best linear correlation. Again, the data is not sufficient to make conclusions but only indicates that such a filter might be an alternative or could be used in parallel with other filtering methods. However, the choice of limit for this filter also influences results and it's not clear how this limit should be selected. Using no filter also seem to imply a linear relation for our data, although with less accuracy. As mentioned in chapter 4.4, The result of Li *et al.* [17] showed that most of the cumulative energy passed the used peak frequency filter. Perhaps a linear model could be accurate enough without using any filter.

Even though there is no evidence proving our models, the limitations need to be discussed to understand how a similar model could be implemented in the future. Some factors that could affect the model include:

- Choice of timing parameters and threshold
- Choice of sensor
- Type of material, dimensions, and layup sequence
- Tensile loading rate [17]
- Type of loading test

Because of these factors, it is likely that a similar model at first can only be used for a specific type of specimen tested under the same conditions. When a model can be proven to be accurate for a specific condition, it needs to be studied how new conditions might affect the model. This knowledge is necessary to understand how acoustic emission can be implemented as a SHM system for composite structures such as a hydrogen tanks. This is important since a structure can be impacted by different loads. For example, a hydrogen tank can be impacted by pressure from hydrogen and fatigue thermal cycling due to variations in temperature. When enough knowledge is acquired for small specimens, further investigations are needed on how to implement the method for large composite structures. Furthermore, other damage types could occur in composite structures making it necessary to understand how acoustic emission can be used to also detect other types of damage.

## 7.5 Future experimental improvements

Further work is needed to understand how acoustic emission could be used to estimate number of matrix cracks in cross-ply CFRP. Here we suggest some improvements that could be made from this study:

- **Sensor choice:** As mentioned in chapter 4.3, sensor resonance negatively impacts the use of peak frequency [7]. Because of this, a sensor with a distinct resonance should be avoided. The bandwidth also needs to be considered. Our sensor sensitivity had a lower limit of 270 kHz which means that frequency content below this limit won't be properly recorded by the sensor. In future studies, a bandwidth with a lower limit of at least 100 kHz should be used.
- **Verification of matrix cracks:** An optical microscope was used to verify the number of matrix cracks for each specimen. This is a very time demanding method and because of this, some other method should be applied to verify the number of cracks in future studies to enable more collection of data.

## 8 Conclusions

This thesis has investigated how acoustic emission could be used to predict the number of matrix cracks in cross-ply CFRP laminates. Experiments were conducted for only one type of layup under the same conditions but with different maximum tensile stress. It's proposed that the number of matrix cracks can be estimated as a linear function of cumulative energy, where the best fit was found when using a high-energy filter and the cumulative energy from the point where the maximum tensile stress is reached. More data is required to validate how accurate such a model is.

The work of this thesis can be used as groundwork for further studies. The data from the results is insufficient in proving reliable methods, but the observations made are worth to further investigate. Further studies are encouraged to investigate how cumulative energy can be used to estimate the number of matrix cracks in composites. When a reliable method is proven for a certain layup and condition, it needs to be investigated how different conditions and layups could influence the method. This is a necessary step in the aim of creating reliable SHM systems for composite structures using acoustic emission.

## 9 References

- [1] C. B. Scruby, "An introduction to acoustic emission," *J. Phys. E: Sci. Instrum.*, vol. 20, no. 8, pp. 946-953, Aug. 1987. doi: 10.1088/0022-3735/20/8/001.
- [2] M. Saeedifar and D. Zarouchas, "Damage characterization of laminated composites using acoustic emission: A review," *Compos. Part B: Eng.*, vol. 195, article 108039, pp. 1-21, Aug. 2020. doi:10.1016/j.compositesb.2020.108039.
- [3] D. Tonelli, M. Luchetta, F. Rossi, P. Migliorino, and D. Zonta, "Structural Health Monitoring Based on Acoustic Emissions: Validation on a Prestressed Concrete Bridge Tested to Failure," *Sensors*, vol. 20, no. 24, article 7272, pp. 1-20, Dec. 2020. doi: 10.3390/s20247272.
- [4] R. Unnithorsson, "Hit Detection and Determination in AE Bursts," in *Acoustic Emission – Res. and App.*, W. Sikorski, Ed., Rijeka, Croatia: InTech, 2013, pp. 1-19. [Online]. Available: [https://www.researchgate.net/publication/245536427\\_Hit\\_Detection\\_and\\_Determination\\_in\\_AE\\_Bursts](https://www.researchgate.net/publication/245536427_Hit_Detection_and_Determination_in_AE_Bursts)
- [5] A. Tillmann, A. Schultz, and J. Campos, "Protocols and Criteria for Acoustic Emission Monitoring of Fracture-Critical Steel Bridges," Minnesota Dept. of Transportation, Minneapolis, Minnesota, USA, pp. 12-16, Tech. Rep. MnDOT 2015-36, June 2015. Accessed: Apr. 14, 2023. [Online]. Available: [https://www.researchgate.net/publication/282912497\\_Protocols\\_and\\_Criteria\\_for\\_Acoustic\\_Emission\\_Monitoring\\_of\\_Fracture-Critical\\_Steel\\_Bridges](https://www.researchgate.net/publication/282912497_Protocols_and_Criteria_for_Acoustic_Emission_Monitoring_of_Fracture-Critical_Steel_Bridges)
- [6] *USB-AE Node<sup>TM</sup> & AEwin<sup>TM</sup> for USB<sup>TM</sup> Software User's Manual*, rev 0, Mistras Group, Princeton, NJ, USA, 2010, pp. 1-29
- [7] O. Z. Moradian and B. Li. (Nov. 2015). Hit Based Acoustic Emission Monitoring of Rock Fractures: Challenges and Solutions. Presented at World Conf. on Acoustic Emission. pp. 1-11 [Online]. Available: [https://www.researchgate.net/publication/301824087\\_Hit\\_Based\\_Acoustic\\_Emission\\_Monitoring\\_of\\_Rock\\_Fractures\\_Challenges\\_and\\_Solutions](https://www.researchgate.net/publication/301824087_Hit_Based_Acoustic_Emission_Monitoring_of_Rock_Fractures_Challenges_and_Solutions)
- [8] N. Godin, P. Reynaud, and G. Fantozzi, "Acoustic Emission: Definition and Overview" in *Acoustic Emission and Durability of Composite Materials*, vol. 3, Hoboken, New Jersey, USA: John Wiley & Sons, Incorporated, 2018. Ch. 1, pp. 1-58. [Online]. Available: <http://ebookcentral.proquest.com/lib/linkoping-ebooks/detail.action?docID=5301760>.
- [9] P. Theobald, B. Zeqiri, and J. Avison. (Sept. 2008). Couplants and Their Influence on AE Sensor Sensitivity. Presented at 28th European Conf. on Acoustic Emission Testing. pp. 13-18 [Online]. Available: <https://www.ndt.net/search/docs.php3?id=14501>
- [10] "Hsu-Nielsen source." NDT.net. <https://www.ndt.net/article/az/ae/hsunielsensource.htm> (accessed June 6, 2023).
- [11] K. Asamene, L. Hudson, and M. Sundaresan, "Influence of attenuation on acoustic emission signals in carbon fiber reinforced polymer panels," *Ultrasonics*, vol. 59, pp. 86–93, May 2015, doi: 10.1016/j.ultras.2015.01.016.

- [12] Z. Hamam, N. Godin, P. Reynaud, C. Fusco, N. Carrere, and A. Doitrand, "Transverse Cracking Induced Acoustic Emission in Carbon Fiber-Epoxy Matrix Composite Laminates," *Materials*, vol. 15, no. 1, article 394, pp. 1-15 Jan. 2022, doi: 10.3390/ma15010394.
- [13] M. S. Loukil, "Experimental and Numerical Studies of Intralaminar Cracking in High Performance Composites," Ph.D. dissertation, dept. of Eng. Sci. and Mathematics, Luleå Univ. of Technology, Luleå, Sweden, 2013. pp. 1-10. [Online]. Available: <http://www.diva-portal.org/smash/record.jsf?pid=diva2%3A999664&dswid=2817>
- [14] J. K. Wells and P. W. R. Beaumont, "Debonding and pull-out processes in fibrous composites," *J. of Materials Sci.*, vol. 20, no. 4, pp. 1275-1284, Apr. 1985. Accessed: June 6, 2023. Available: <https://link.springer.com/article/10.1007/BF01026323>
- [15] F. E. Oz, N. Ersoy, M. Mehdikhani, and S. V. Lomov, "Multi-instrument in-situ damage monitoring in quasi-isotropic CFRP laminates under tension," *Compos. Struct.*, vol. 196, pp. 163–180, July 2018, doi: 10.1016/j.compstruct.2018.05.006.
- [16] C. Baker, G. N. Morscher, V. V. Pujar, and J. R. Lemanski, "Transverse cracking in carbon fiber reinforced polymer composites: Modal acoustic emission and peak frequency analysis," *Compos. Sci. and Technol.*, vol. 116, pp. 26–32, Sept. 2015, doi: 10.1016/j.compscitech.2015.05.005.
- [17] X. Li, M. Saeedifar, R. Benedictus, and D. Zarouchas, "Damage accumulation analysis of cfrp cross-ply laminates under different tensile loading rates," *Compos. Part C: Open Access*, vol. 1, article 100005, pp. 1-14, Aug. 2020, doi: 10.1016/j.jcomc.2020.100005.
- [18] "Acoustic Emission Source Location Techniques." nde-ed.org. [https://www.nde-ed.org/NDETechniques/AcousticEmission/AE\\_SourceLocation.xhtml](https://www.nde-ed.org/NDETechniques/AcousticEmission/AE_SourceLocation.xhtml) (Accessed June 7, 2023)
- [19] F. Ciampa and M. Meo, "A new algorithm for acoustic emission localization and flexural group velocity determination in anisotropic structures," *Comp. Part A: Appl. Sci. and Manuf.*, vol. 41, no. 12, pp. 1777-1786, Dec. 2010, doi: 10.1016/j.compositesa.2010.08.013
- [20] S. K. Al-Jumaili, M. R. Pearson, K. M. Holford, M. J. Eaton, and R. Pulin, "Acoustic emission source location in complex structures using full automatic delta T mapping technique," *Mech. Syst. And Signal Proc.*, vol. 72-73, pp. 513-524, May 2016, doi: 10.1016/j.ymssp.2015.11.026
- [21] E. Berggren, D. Mansoob, and D. Söderkvist, "Manufacturing and Damage Analysis of Prepreg Carbon Fibre Reinforced Epoxy Composite," 2023, unpublished, Linköping university, LIU-IEI-TEK-G--23/02189--SE.
- [22] I. E. Tabrizi, R.M.A Khan, E. Massarwa, J.S.M Zanjani, H.Q Ali, E. Demir, and M. Yildiz, "Determining tab material for tensile test of CFRP laminates with combined usage of digital image correlation and acoustic emission techniques," *Compos. Part A: Appl. Sci. and Manuf.*, vol. 127, article 105623, pp. 1-13, Dec. 2019, doi: 10.1016/j.compositesa.2019.105623.



## 10 Appendix

The raw data and the MatLab script used for data analysis and figure plotting can be found at:

<https://github.com/QQalle/AE-Waveform-crack-detection>